Evaluation of Displacement-Based Analysis and Design Methods for Steel Frames with Passive Energy Dissipators

by

M.S. Williams[1] and F. Albermani[2]

Civil Engineering Research Bulletin No. 24

University of Queensland
Department of Civil Engineering
Hawken Engineering Building
Brisbane, Queensland 4072
Australia

ISBN 186 499 7540

[1] Visiting from: University of Oxford, Department of Engineering Science, Parks Road, Oxford OX1 3PJ, UK.
Email: martin.williams@eng.ox.ac.uk
[2] Email: f.albermani@uq.edu.au

Abstract

This report investigates the use of displacement-based, or *pushover* methods of analysis in the design of frames incorporating passive dissipative devices. An extensive analysis and design study of 3-, 6- and 10-storey frames, both undamped moment-resisting frames (MRFs) and retrofitted with hysteretic and frictional dissipators has been performed. Frames were modelled using the finite element program Sap2000 and were analysed using both non-linear static pushover analysis and non-linear time history analysis. The principal aims were to assess the degree of improvement in performance achieved through use of the devices, and the suitability of various displacement-based analysis methods for estimating the seismic response of frames fitted with dissipative devices.

It was found that both dissipative systems led to substantial improvements in frame performance, in terms of plastic hinge formation (reduced to virtually zero) and deformation (reduced by a factor of more than 2). Base shears remained similar to those for the undamped MRFs.

Pushover analyses were found to be a useful design tool for the unretrofitted frames, giving good estimates of the overall displacement demands, base shears and plastic hinge formation. However, the various pushover approaches proved less successful at estimating the performance of the dissipative frames, where they appeared to underestimate the beneficial effects of energy dissipation.

Of the various pushover methods assessed, the FEMA 356 approach appears to offer the most accurate and realistic estimate of seismic performance, with the exception of the inter-storey drift distribution.

For the 6- and 10-storey frames (both ductile MRFs and dissipative frames), pushover methods using fixed, single load patterns gave rather poor estimates of the distribution of inter-storey drift with height. Far better drift estimates were obtained using the modal pushover method, in which pushover results obtained using force distributions based on the first three modes are combined by the SRSS method.

Acknowledgements

The work described in this report was conducted while the first author was an academic visitor at the University of Queensland, between July and December 2003. We are grateful to the Head of the Civil Engineering Department, Associate Professor Peter Dux, and the Dean of the Engineering, Physical Sciences and Architecture Faculty, Professor Michael Kenniger, for their help and support in arranging this visit. The generous financial support provided by the UK's Royal Academy of Engineering under the grant "Dissipative devices in seismic design" is also gratefully acknowledged.

Some of the framed structures used in the evaluations were based on designs created by the undergraduate thesis group of Daniel Chambers, Debbie Macmillan and Daniel Moore. Their hard work is warmly acknowledged.

Contents

Abstract 2

Acknowledgements 3

Contents 4

1. Introduction 5

2. Selection of Dissipator Types 5

3. Design Parameters 8

   3.1 Response spectrum 8
   3.2 Generation of spectrum-compatible accelerograms 9

4. Building Designs 9

   4.1 Moment resisting frames 9
   4.2 Dissipative frames 13

5. Analysis and Design Methods 15

   5.1 Modelling of the Structure 15
   5.2 Modelling of the Dissipators 15
   5.3 Pushover Analysis Methods 16
   5.4 Simple Design Methods for Frames with Dissipators 23
   5.5 Time History Analysis 24

6. Results 24

   6.1 Natural Period 24
   6.2 Target Displacements 25
   6.3 Base Shear 28
   6.4 Plastic Hinge Formation 30
   6.5 Inter-StoreyDrifts 30
   6.6 Link Deformations 41

7. Conclusions 41

References 43

Appendix A. Spectrum-Compatible Time Histories A1

1. Introduction

Passive dissipative devices have the potential to provide significant improvements to the seismic performance of structures without the need for the sophisticated technology and cost associated with active control systems. In recent year numerous different dissipative systems have been proposed and some structures have been built or retrofitted with such devices. Most devices dissipate energy through one of three mechanisms – hysteresis, friction or viscous damping. In all cases their behaviour is, of course, highly non-linear.

At the same time, approximate displacement-based methods of seismic design, based on the use of non-linear static *pushover* analysis, have undergone a rapid increase in popularity and are starting to find their way into design guides and codes of practice. Several different approaches exist, based on different levels of simplification, and no consensus has yet emerged as to the most convenient or reliable method.

This report brings together these two important topics by assessing the suitability of pushover methods for the analysis and design of frames incorporating passive dissipative devices. A series of analyses of steel framed structures, with and without the addition of passive dissipative devices, have been performed using the program Sap2000 (CSI, 2002). The principal aims are to assess (a) the degree of improvement in performance achieved through use of the devices, and (b) the suitability of various displacement-based analysis methods for estimating the seismic response of frames fitted with dissipative devices.

Dissipator properties are briefly discussed in Chapter 2. Chapters 3 and 4 then present the design criteria adopted and he building designs chosen for the study. Chapter 5 describes the different analysis approaches used and Chapter 6 presents comparisons between the various methods.

2. Selection of Dissipator Types

A very wide range of passive dissipative devices exists or has been proposed. Substantial reviews have been published by Constantinou et al (1998) and Soong and Spencer (2002). The major categories of device are:

• Hysteretic devices based on metallic yielding – examples include the ADAS (Added Damping And Stiffness) device (Aiken and Kelly, 1992) and the knee element (Aristazabal-Ochoa, 1986; Williams et al., 2002). A companion report to this one (Williams and Albermani, 2003) describes tests on a simple yielding shear panel device, based on an unpublished proposal by Dorka. Obviously these elements are elastic up to yield and then generally display a typical steel hysteresis loop, often with significant strain hardening, such as that shown in Figure 2.1 for a knee element.

• Frictional systems such as the well-known Pall damper (Pall and Marsh, 1982), which comprises a series of clamped plates surfaced with brake lining material. These are generally taken to be rigid up to their slip load, then to slip at constant load. Figure 2.2 shows the results of experiments on a similar device achieved by Wu at al (2003). However, Wu et al. have also shown that, due to geometric non-linearities in the devices, brace forces may increase significantly after slip.

• Solid visco-elastic dampers (e.g. Xu and Zhang, 2001), in which materials such as acrylic copolymers are bonded between steel plates and dissipate energy through shear deformation as the plates move. These materials have no activation level and exhibit elliptical hysteresis loops, Figure 2.3.

• Fluid viscous dampers, which generally comprise non-linear stiffness and damping components. For example, the French company Jarret Devices quote the following governing equations for their dampers:

$$F = F_d + F_e \tag{2.1}$$

$$F_d = c\,\mathrm{sgn}(\dot{x})\,|\dot{x}|^{\alpha} \tag{2.2}$$

$$F_e = k_2 x + \frac{(k_1 - k_2)x}{\left[1 + \left|\frac{k_1 x}{F_0}\right|^{R}\right]^{1/R}} \tag{2.3}$$

where c is a damping coefficient with units of kN(s/mm)$^{\alpha}$, the exponent α takes a value between 0.1 and 0.2, k_1 and k_2 are the initial and post-yield stiffnesses, F_0 is the pre-load and the exponent R is usually taken as 5. Figure 2.4 shows plots of the resulting hysteresis loops for two different values of pre-load: with a large pre-load the bilinear stiffness is clearly evident, while with a very small pre-load the second term in Equation (2.3) becomes negligible and only the post-yield stiffness is evident. In each plot hysteresis curves are shown for several different rates of sinusoidal loading – it can be seen that, because of the low value of α, the response is not particularly rate-sensitive.

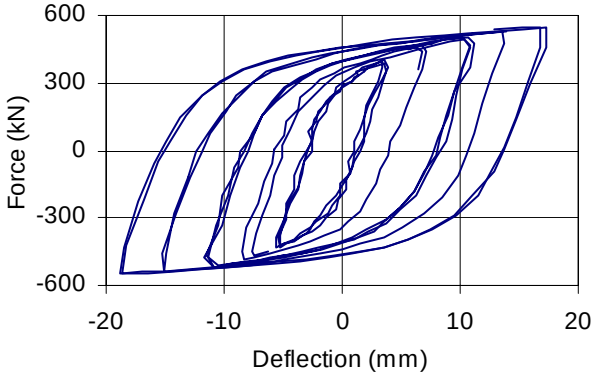

Figure 2.1
Hysteresis of 152×152×30UC knee element

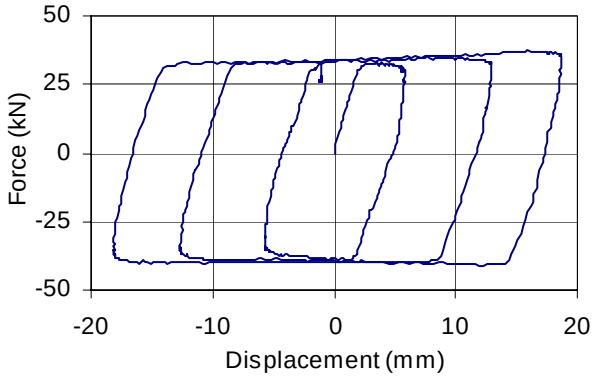

Figure 2.2
Hysteresis of Pall-type friction element

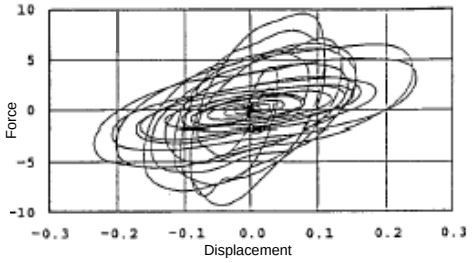

Figure 2.3 Hysteresis of solid visco-elastic damper (after Xu and Zhang, 2001)

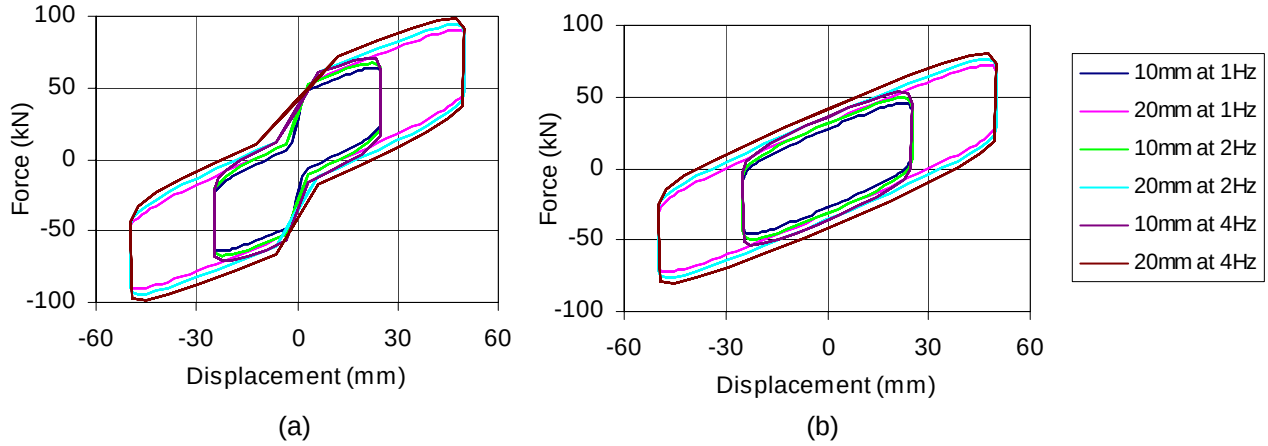

Figure 2.4 Hysteresis of Jarret fluid viscous damper: (a) with high preload, (b) with negligible preload

Initially it was intended to include three different types of dissipator in the study: hysteretic, frictional and fluid viscous. The latter was felt to be particularly significant since its obvious (if limited) velocity dependence calls into question the appropriateness of using a non-linear static analysis as the basis for design. At this stage, however, only hysteretic and frictional devices have been analysed, partly due to time constraints and partly due to apparent bugs in the damper element in Sap2000.

Hysteretic devices were based on the knee element, which spans diagonally across a beam-column joint and connects to a diagonal brace as shown in Figure 2.5(a). The K-brace configuration was chosen as previous studies suggest this provides the optimal combination of energy dissipation and drift limitation. Knee element properties were based on a tri-linear idealisation of the hysteresis curve presented in Figure 2.1. A series of idealised knee elements was designed with designations *ke300*, *ke350*, *ke400*…, where the number refers to the initial yield load in kN. Details of the modelling of the devices are given in Section 5.2.

Frictional devices were of the Pall type, positioned at the centre of an X-brace, Figure 2.5(b). Properties were based on a rigid-plastic idealisation of the hysteresis shown in Figure 2.2. Filiatrault and Cherry (1987) have shown that this formulation is only strictly correct if the device slips during every cycle of loading, but it is considered sufficiently accurate for this study. Also, the geometric non-linearity referred to above has not been modelled at this stage. A series of idealised friction elements were designed with designations *fric300*, *fric400*…, where the number refers to the slip load in kN.

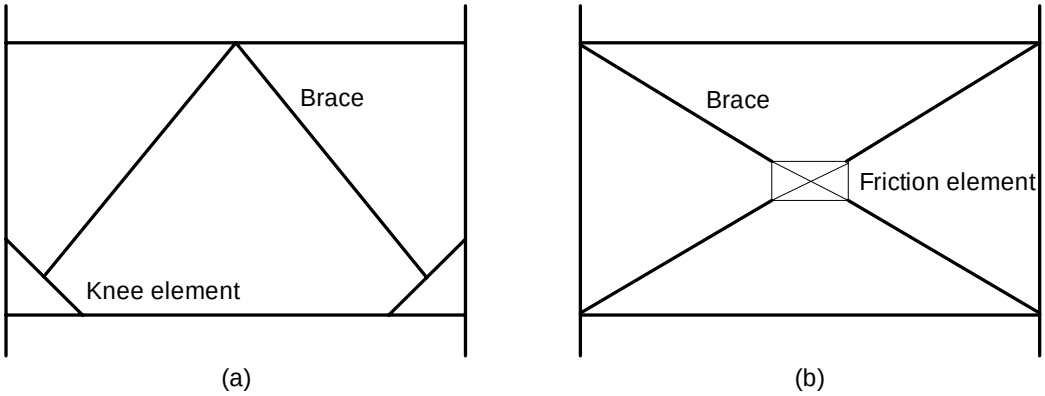

Figure 2.5 Dissipative frame layouts: (a) knee braced frame, (b) friction-damped frame

3. Design Parameters

The frames presented in Section 4 below were initially designed to two different codes of practice – the NEHRP (1997) provisions and the Australian seismic code AS 1170.4 (1993). However, for the purposes of the analyses and assessments performed here, it was decided to use a single earthquake specification, taken from the European code EC8 (2003). This gives a slightly more sophisticated definition of the design earthquake than either of the other codes, and provides a point of comparison that is independent of the original design basis of any of the structures.

3.1 Response spectrum

Buildings were designed, analysed and assessed against the EC8 (2003) Type 1 design spectrum (for moderate or large events), soil type C (dense sand or gravel, or stiff clay), scaled to a peak ground acceleration of 3.5 m/s^2. This represents a reasonably large earthquake in Europe or the USA, and an exceptionally large event in Australia. The spectrum is shown in Figure 3.1, both in the conventional acceleration vs period format, and in the ADRS (acceleration-displacement) format used by ATC 40 (1996).

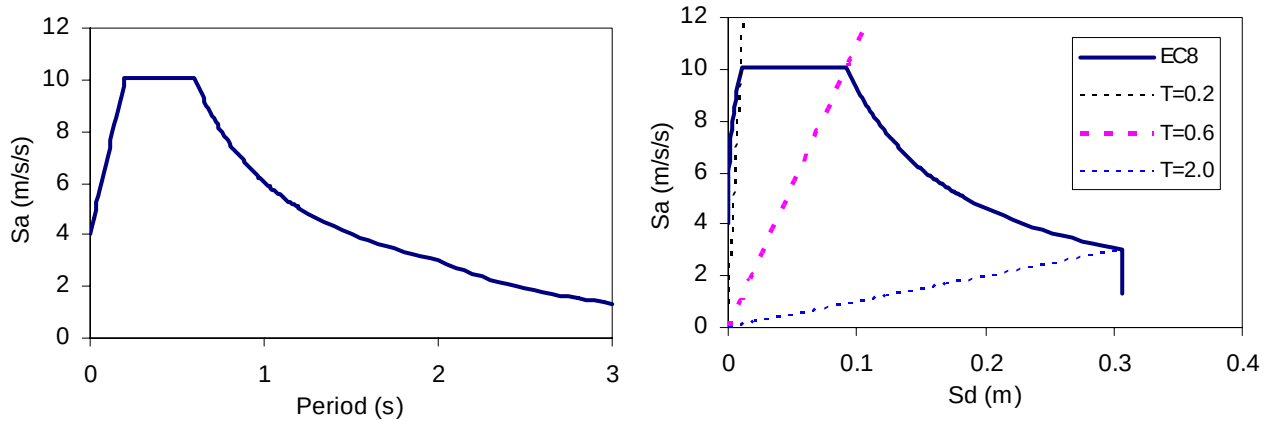

Figure 3.1 EC8 design spectrum plotted in conventional and ADRS formats

3.2 Generation of Spectrum-Compatible Accelerograms

For time history analysis, an ensemble of 30 acceleration time histories compatible with the response spectrum of Figure 3.1 was created using the program Simqke (Gasparini and Vanmarcke, 1976). To create a reasonably harsh, long-duration event, a total duration of 20 seconds was specified, comprising a 2 second rise time, 10 seconds of strong motion and an 8 second decay.

Details of the generation process, plots of the accelerograms and comparisons with the target spectrum can be found in Appendix A.

4. Building Designs

This section presents the designs of all the buildings chosen for analysis. Four basic buildings were chosen/designed: 3-, 6- and 10-storey ductile moment resisting frames (MRFs), and a 10-storey elastic MRF. Each of the ductile frames was then modified by the addition of bracing and dissipative elements (both hysteretic and frictional), giving a total of six dissipative structures.

4.1 Moment Resisting Frames

The 3-storey frame design was taken from the work of Ramirez et al. (2001). It was designed using the American NEHRP (1997) guidelines for a peak ground acceleration of 0.4g with a response modification (ductility) factor of $R = 8$, and standard American section sizes. In plan the building consists of five 8.23 m bays in each direction. Storey heights are 4.42 m at the first floor and 4.3 m at the upper floors. Lateral loads are resisted by three-bay special moment resisting frames on each side of the building. The structural details are shown in Figure 4.1. The building has a fundamental period of 1.1 s – this is very long for a 3-storey frame and perhaps rather unrealistic, but it is likely to provide a good test of the various pushover analysis methods.

The 6-storey frame design was also taken from Ramirez et al. (2001). It has a very similar layout and the same design criteria as the 3-storey frame. The structural details are shown in Figure 4.2. The building has a fundamental period of 1.9 s, again rather long for a frame of this height.

The 10-storey frames were loosely based on designs produced by a UQ undergraduate thesis group under the authors' guidance. They were designed in accordance with the Australian seismic code AS 1170.4 (1993) for a peak ground acceleration of 0.33g, using standard Australian sections (which are similar to British ones). Two buildings were designed, with ductility factors of $R = 1$ and $R = 4.5$. The buildings consist of three 6 m bays in each direction, with 4 m storey heights. The structural details are shown in Figure 4.3. The $R = 1$ building has a natural period of 1.2 s and the $R = 4.5$ building has a natural period of 2.4 s.

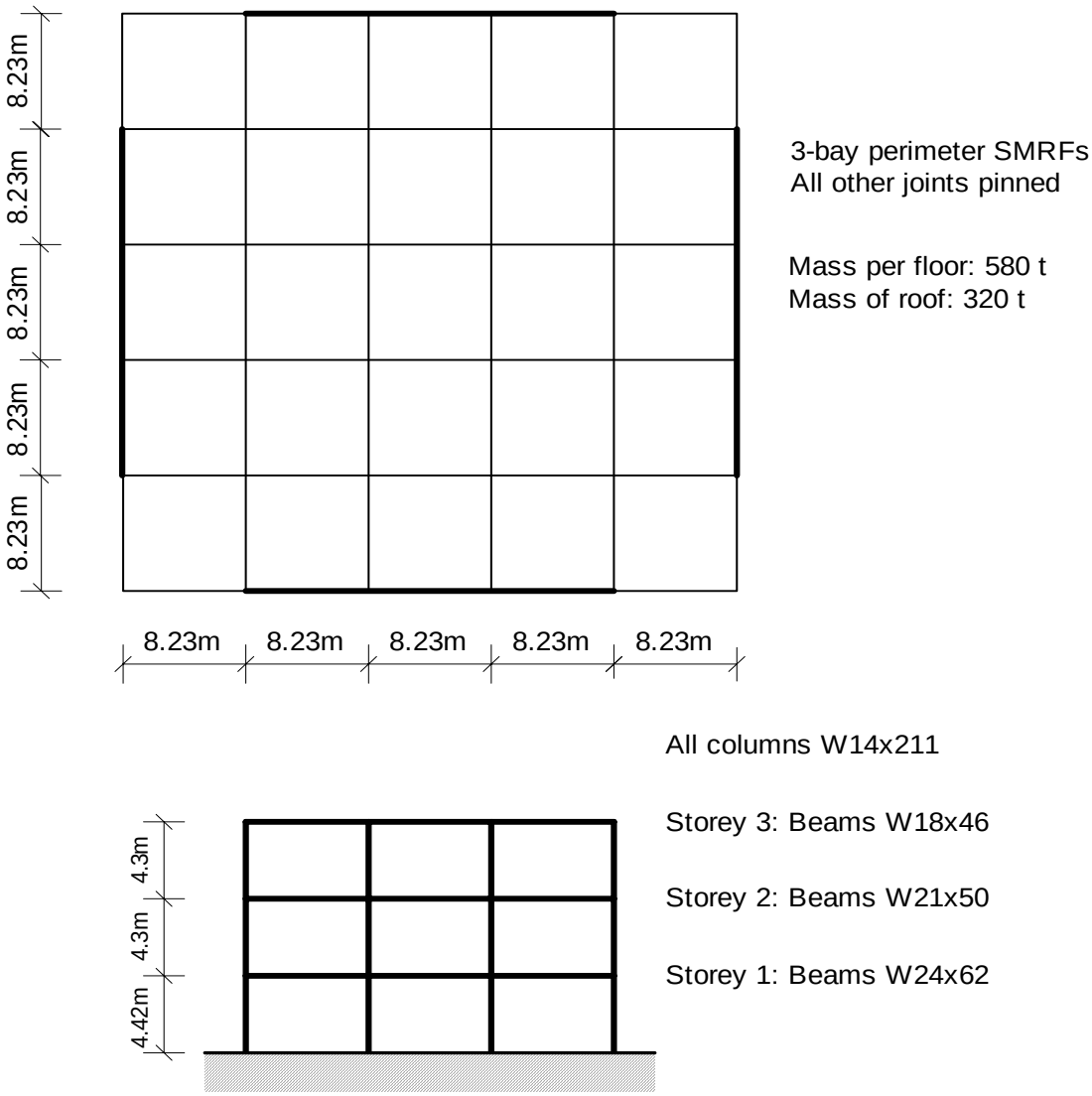

Figure 4.1 Structural details of 3-storey MRF

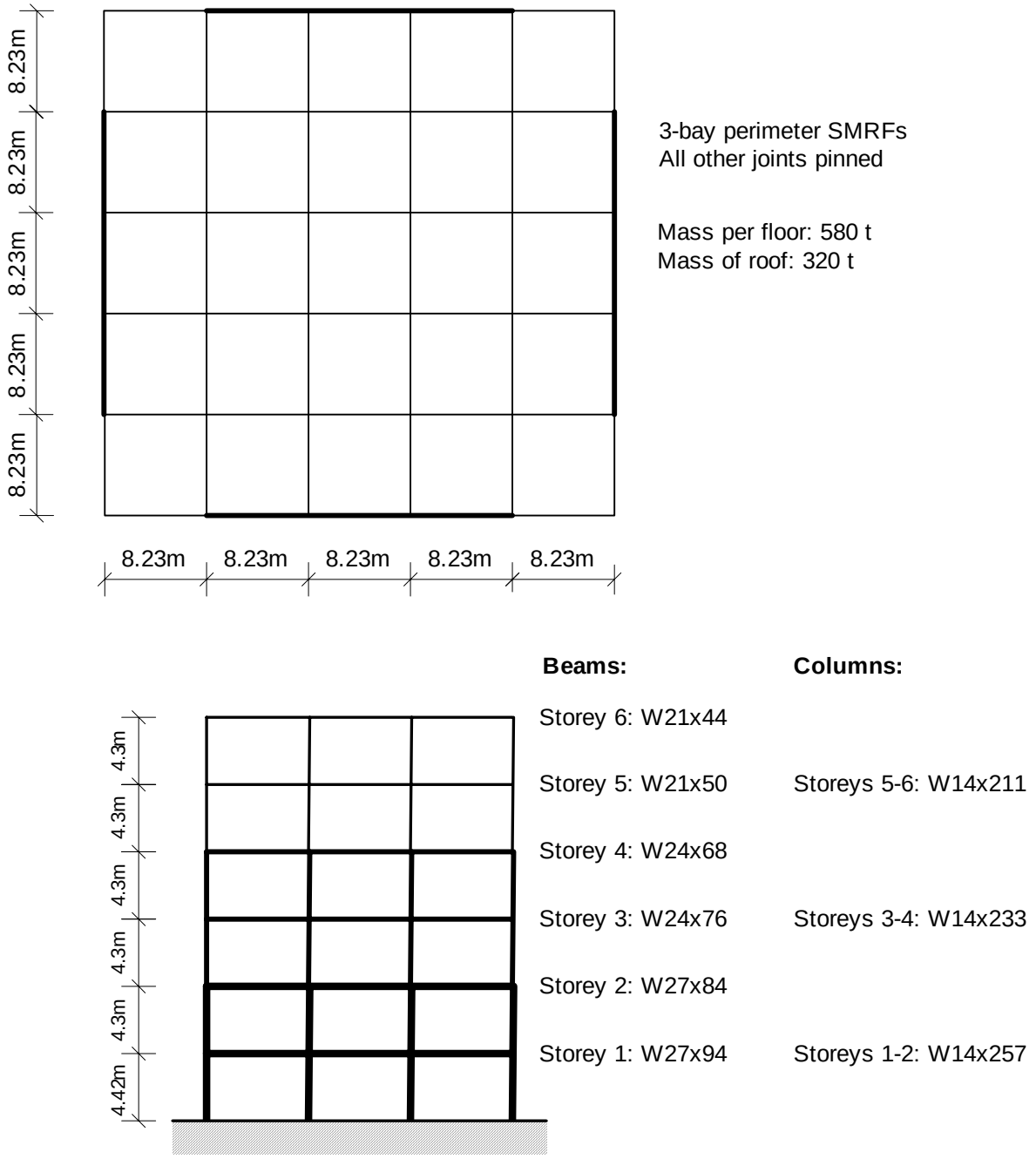

Figure 4.2 Structural details of 6-storey MRF

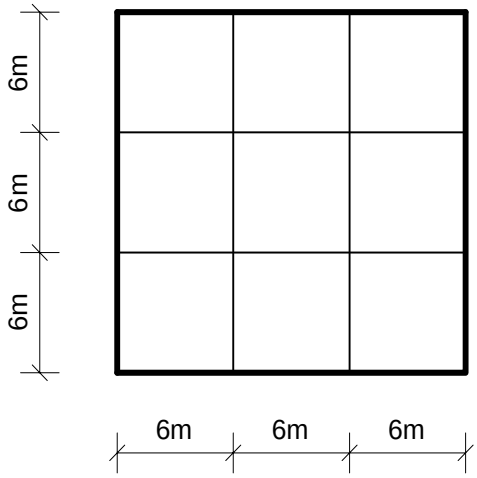

Perimeter MRF
Internal joints pinned

Mass per floor: 195 t
Mass of roof: 156 t

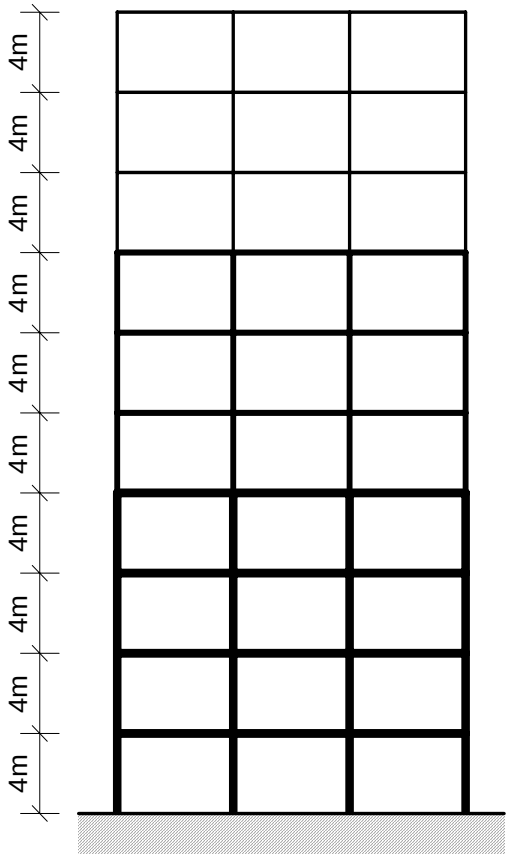

	R = 4.5:	**R = 1.0:**
Storeys 8 - 10	Beams: 460UB67.1 Columns: 310UC118	Beams: 530UB92.4 Columns: 400WC361
Storeys 5 - 7	Beams: 530UB92.4 Columns: 350WC197	Beams: 800WB192 Columns: 500WC414
Storeys 1 - 4	Beams: 610UB101 Columns: 350WC280	Beams: 900WB218 Columns: Proprietary

Figure 4.3 Structural details of 10-storey MRFs

4.2 Dissipative frames

The dissipative frames were designed as retrofits to the ductile moment-resisting frames, i.e. bracing and dissipative elements were added to the frames so as to improve their performance, with no attempt made to redesign the main frame elements. In each case the design aims were to convert a ductile frame into one in which the main members stayed as near to elastic as possible while the dissipators suffered no ultimate failure (defined as exceeding a limiting deformation) under the design earthquake, as specified in Section 3.1. For the knee elements, failure was defined as occurring when the extension of a link element representing the combination of a brace and knee element exceeded 40 mm (corresponding to a knee element deformation of 25 mm). For the friction elements, failure was assumed to occur when a link representing a brace and a friction element exceeded 30 mm (virtually all in the friction element).

Initial rough sizing of the dissipative elements was performed using the two approximate design methods set out in Section 5.4 below, while final design was based on pushover analysis using the FEMA 356 (2000) approach, as described in Section 5.3.

The dissipator designs and initial elastic periods of the retrofitted buildings are set out in Figures 4.4 – 4.6. The designation *ke300* refers to a knee element with in initial yield load of 300 kN. Similarly, *fric300* refers to a friction element with a slip load of 300 kN. Braces were sized to carry the maximum load in the adjoining dissipator with a factor of safety of 2.0 on yield.

The design objective of no yield in the main frame was not achieved in all cases. It was found that a point was reached where increasing the dissipator capacity had no beneficial effect, and in some cases was even detrimental. In general, the friction damped frames came closer to meeting the design objective than the knee braced frames.

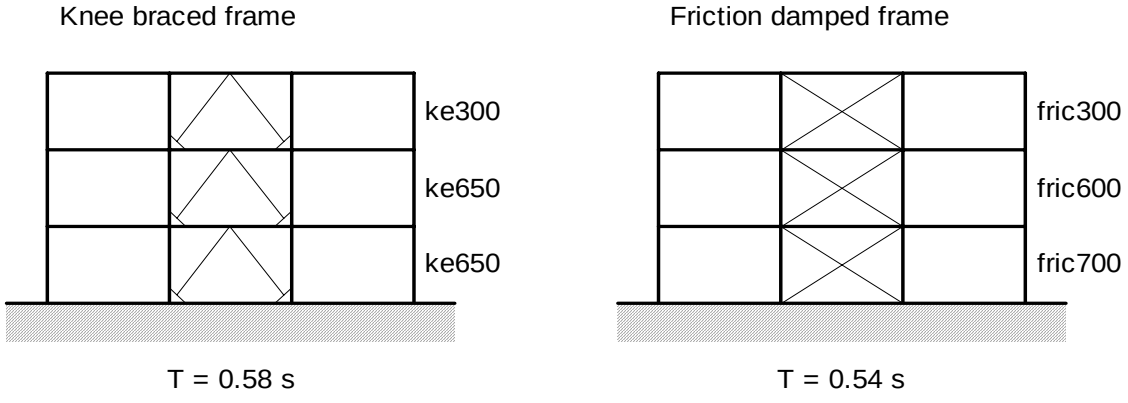

Figure 4.4 Dissipator designs for 3-storey frames

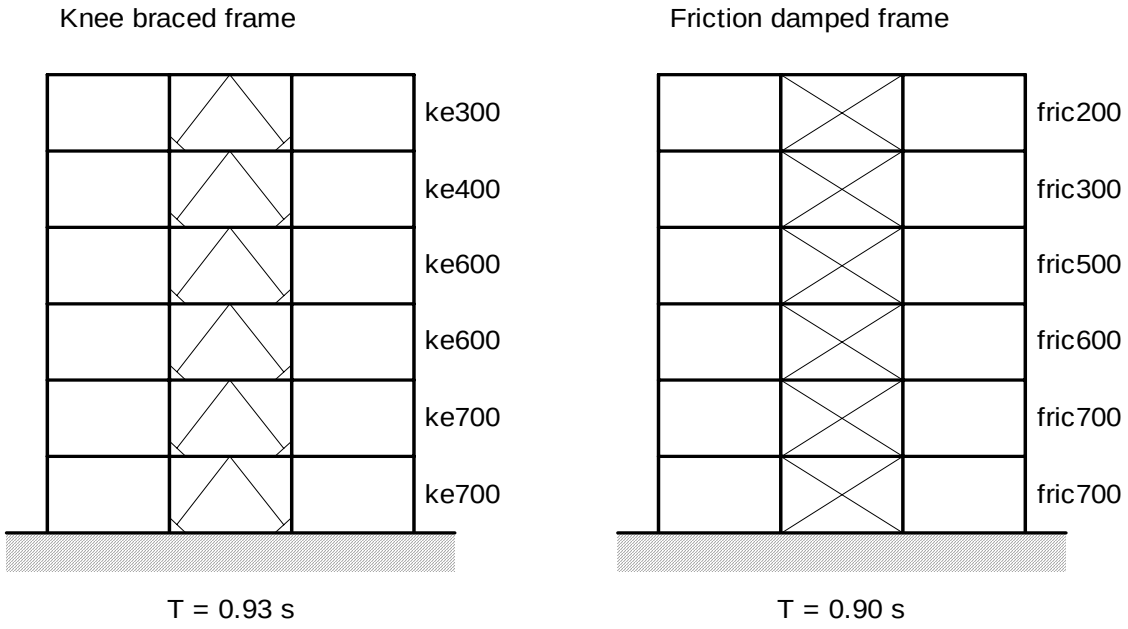

Figure 4.5 Dissipator designs for 6-storey frames

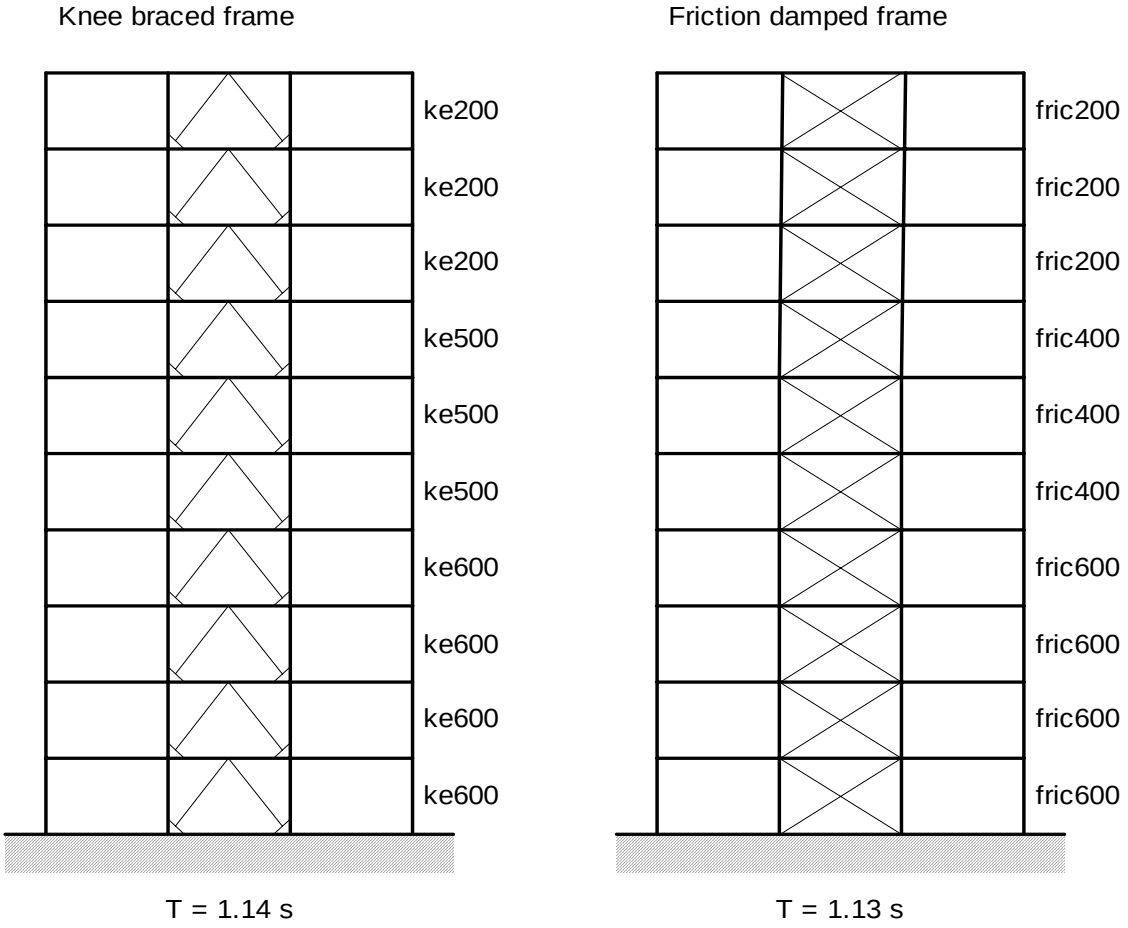

Figure 4.6 Dissipator designs for 10-storey frames

5. Analysis and Design Methods

In this section the modelling of the frames using Sap2000 is discussed, as are the various pushover analysis methods investigated and the non-linear time history analysis with which the results are compared.

5.1 Modelling of the Structure

In each case, only a single, planar MRF was modelled. The beams and columns were modelled using standard frame elements in Sap. Elements were assumed to behave linearly except at pre-defined hinge locations, which were located at 5% of the length from each end of each member. Hinges were assigned a 5% strain hardening ratio and were assumed to fail completely at a rotational ductility of 6. Floors were assumed to act as rigid diaphragms and to distribute their mass uniformly on the supporting beams.

5.2 Modelling of the Dissipators

Knee element hysteretic properties were based on a tri-linear idealisation of the hysteresis curve as shown in Figure 5.1(a). In order to come up with a series of simple, idealised knee element properties, it was assumed that both strength and stiffness could be scaled in the same way for different knee element sizes, so that only the yield forces varied between sections, not the yield deformations. This is not strictly correct, but the error thus introduced is likely to be small.

The brace connected to a knee element was designed to carry the maximum knee element force with a factor of safety of 2 against yielding, assuming mild steel with a yield strength of 300 MPa. Braces were assumed not to buckle. For modelling in Sap, a single link element was defined representing the combined stiffness of the elastic brace and the yielding knee element acting in series. Figure 5.1(b) shows the skeleton curves for a typical knee element and the corresponding knee/brace link element in a direction along the brace axis.

A similar approach was adopted for modelling the friction elements, except that the initial idealisation was simply to elastic-perfectly plastic. Typical curves are shown in Figure 5.2.

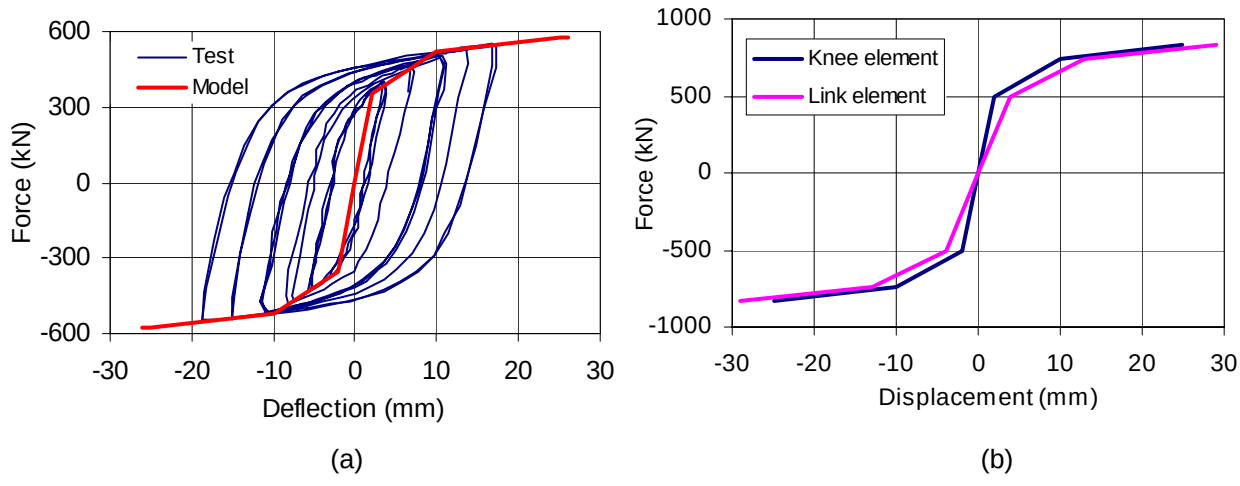

Figure 5.1 Modelling of a knee element: (a) Idealisation of hysteresis data, (b) typical skeleton curves for a ke500 element and the corresponding ke/brace link element in the 10-storey frame

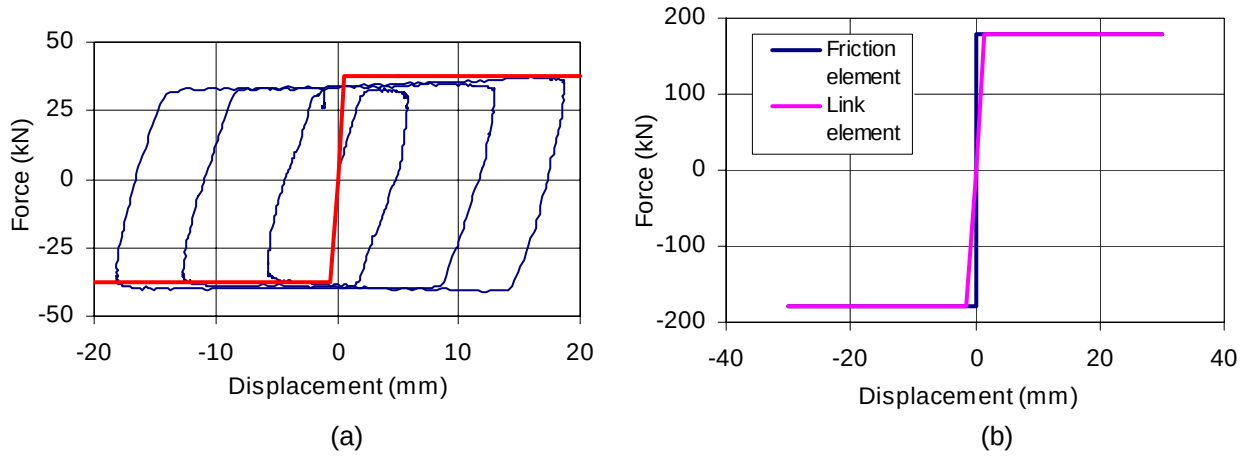

Figure 5.2 Modelling of a friction element: (a) Idealisation of hysteresis data, (b) typical skeleton curves for a fric300 element and the corresponding element/brace link element in the 10-storey frame

5.3 Pushover Analysis Methods

Displacement-based design methods make use of non-linear static, or *pushover*, analysis (Fajfar and Fischinger, 1988; Lawson et al. 1994; Krawinkler and Seneviratna, 1998). Appropriate lateral load patterns are applied to a numerical model of the structure and their amplitude is increased in a stepwise fashion. A non-linear static analysis is performed at each step, until the building fails. A pushover curve (base shear against top displacement) can then be plotted. This is then used together with the design response spectrum to determine the top displacement under the design earthquake – termed the *target displacement* or *performance point*. The non-linear static analysis is then revisited to determine member forces and deformations at this point.

These methods are considered a step forward from the use of linear analysis and ductility-modified response spectra, because they are based on a more accurate estimate of the distributed yielding within a structure, rather than an assumed, uniform ductility. The generation of the pushover curve also provides the engineer with a good feel for the non-linear behaviour of the structure under lateral load. However, it is important to remember that pushover methods have no rigorous theoretical basis, and may be inaccurate if the assumed load distribution is incorrect. For example, the use of a load pattern based on the fundamental mode shape may be inaccurate if higher modes are significant, and the use of a any fixed load pattern may be unrealistic if yielding is not uniformly distributed, so that the stiffness profile changes as the structure yields.

The main differences between the various proposed methods are (i) the choices of load patterns to be applied and (ii) the method of simplifying the pushover curve for design use. The methods used in this study are summarised below.

5.3.1 EC8 (2003)

1. Pushover analysis – apply the following two load patterns:

   Modal – the acceleration distribution is assumed proportional to the fundamental mode shape. The inertia force F_i on mass i is then:

$$F_i = \frac{m_i \phi_i}{\sum_{j=1}^{n} m_j \phi_j} F_b \tag{5.1}$$

   where F_b is the base shear, m_i the ith storey mass and ϕ_i the mode shape coefficient for the ith floor. If the fundamental mode shape is assumed linear then ϕ_i is proportional to storey height h_i and Equation (5.1) can be written as:

$$F_i = \frac{m_i h_i}{\sum_{j=1}^{n} m_j h_j} F_b \tag{5.2}$$

   Uniform – the acceleration is assumed constant with height. The inertia forces are then given by:

$$F_i = \frac{m_i}{\sum_{j=1}^{n} m_j} F_b \tag{5.3}$$

   Plot pushover curve F_b vs d, with maximum displacement d_m.

2. Convert pushover curves to equivalent SDOF system using:

$$F^* = \frac{F_b}{\Gamma} \tag{5.4}$$

$$d^* = \frac{d}{\Gamma} \tag{5.5}$$

$$\Gamma = \frac{\sum_{j=1}^{n} m_j \phi_j}{\sum_{j=1}^{n} m_j \phi_j^2} \tag{5.6}$$

3. Simplify to elastic-perfectly plastic as shown in Figure 5.3. Set F_y^* equal to maximum load, choose d_y^* to give equal areas under actual and idealised curves.

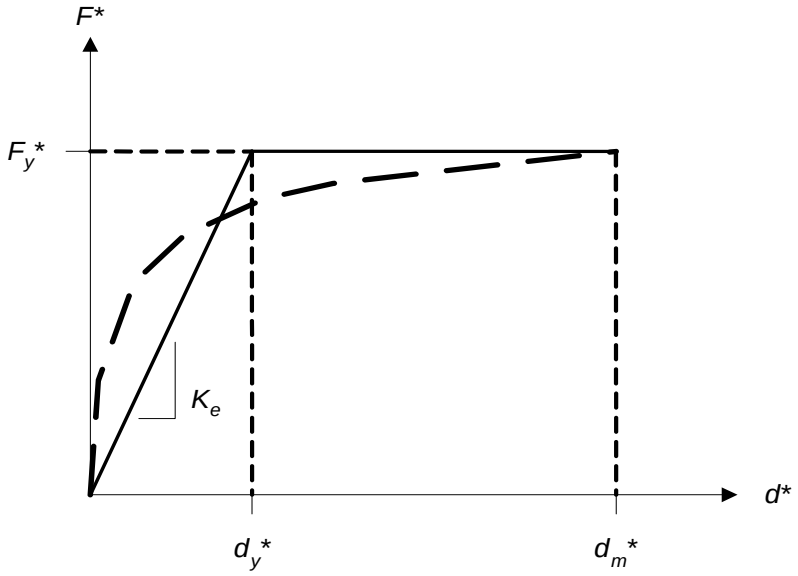

Figure 5.3 Idealisation of pushover curve in EC8

4. Calculate target displacement of SDOF system under design earthquake:

$$d_t^* = S_a \frac{T^2}{4\pi^2} \qquad T \geq T_c \tag{5.7}$$

$$d_t^* = S_a \frac{T^2}{4\pi^2} \frac{1}{q}\left[1 + (q-1)\frac{T_c}{T}\right] \qquad T < T_c \tag{5.8}$$

where

$$q = \frac{S_a}{(F_y^* / m^*)} \tag{5.9}$$

$$m^* = \sum_{j=1}^{n} m_j \phi_j \tag{5.10}$$

T is the elastic period of the idealised SDOF system, S_a is the spectral acceleration corresponding to T, and T_c is the corner period of the design response spectrum, i.e. the period at the transition between the constant acceleration and constant velocity parts of the curve.

5. Transform target displacement back to that of the original MDOF system using Equation (5.5).

6. Check that $d_t \leq d_m/1.5$. Check member strengths and storey drifts are acceptable at this value of d_t.

5.3.2 FEMA 356 (2000)

1. Pushover analysis – apply the following two load patterns:

   Modal – use either an acceleration distribution proportional to the fundamental mode shape or a multi-modal load distribution obtained from a response spectrum analysis. If using the fundamental mode shape, the inertia force distribution is given by Equation (1). The fundamental mode shape can be obtained from a modal analysis, or an assumed shape can be used, giving the load distribution:

$$F_i = \frac{m_i h_i^k}{\sum_{j=1}^{n} m_j h_j^k} F_b \tag{5.11}$$

$$\begin{aligned} k &= 1.0 && T \le 0.5\text{s} \\ &= 0.75 + \frac{T}{2} && 0.5 \le T \le 2.5s \\ &= 2.0 && 2.5 \le T \end{aligned} \tag{5.12}$$

   Either uniform or adaptive – For the uniform pattern the inertia forces are then given by Equation (5.3).

   Plot pushover curve F_b vs d, with maximum displacement d_m.

2. Simplify to bilinear as shown in Figure 5.4. Choose parameters so as to give approximately equal areas under actual and idealised curves. Initial stiffness estimate is governed by the requirement that the actual and idealised curves intersect at $0.6F_y$. Post-yield stiffness is governed by the requirement for the curves to meet at the target displacement. This may require some iteration since d_t is not determined until later.

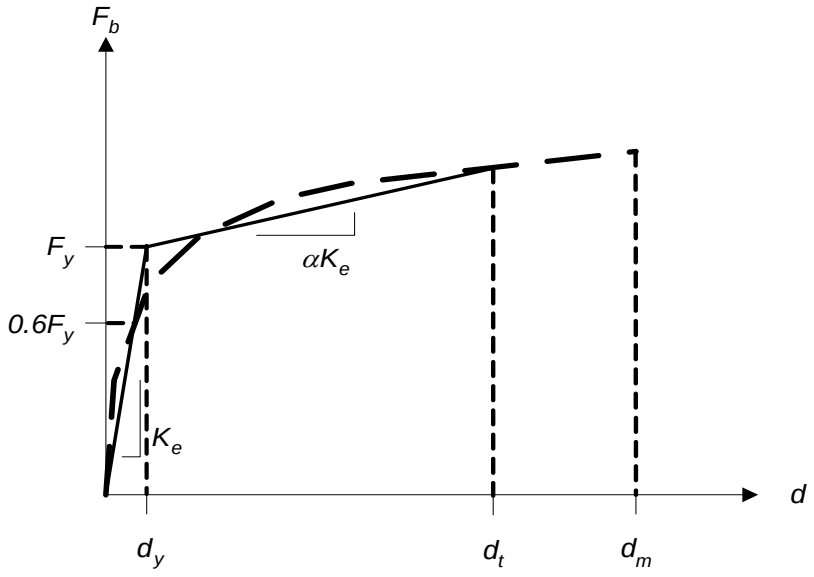

Figure 5.4 Idealisation of pushover curve in FEMA 356

3. Calculate target displacement of MDOF system under design earthquake:

$$d_t = \Gamma S_a \frac{T_e^2}{4\pi^2} \qquad T_e \geq T_c \tag{5.13}$$

$$d_t = \Gamma S_a \frac{T_e^2}{4\pi^2} \frac{1}{q}\left[1 + (q-1)\frac{T_c}{T_e}\right] \qquad T_e < T_c \tag{5.14}$$

T_e is the elastic period of the idealised MDOF system and S_a is the spectral acceleration corresponding to T_e.

4. Check member strengths and storey drifts are acceptable at this value of d_t.

Note: The main calculation steps are equivalent to the EC8 procedure. The significant differences are (a) a slightly wider choice of load patterns and (b) a more realistic idealisation of the pushover curve.

5.3.3 Modal pushover (Chopra and Goel, 2002, Chintanapakdee and Chopra, 2003)

Proposed as a modification to the FEMA method outlined above.

1. Pushover analysis – apply modal load patterns corresponding to the first three mode shapes as determined by eigenvalue analysis. Inertia loads are given by Equation (5.1).

   Plot pushover curve F_b vs d, with maximum displacement d_m.

2. Simplify to bilinear as in FEMA 356 – see Figure 5.4 above.

3. Calculate target displacement of MDOF system under design earthquake as in FEMA 356 – see Equations (5.13) and (5.14) above.

4. Calculate storey drifts, member loads etc for this target displacement. Combine results for each mode by SRSS method.

5.3.4 Capacity spectrum (ATC 40, 1996)

1. Perform pushover analysis as for EC8, using load distributions given by Equations (5.1) and (5.3).

2. Convert pushover curve to *capacity spectrum*, plotted in acceleration-displacement response spectrum (ADRS) format:

$$S_a = \frac{F_b}{\alpha W} \tag{5.15}$$

$$S_d = \frac{d}{\Gamma \phi_n} \tag{5.16}$$

where W is the total weight of the building, ϕ_n is the mode shape coefficient at the location where d is measured (normally the roof) and the modal mass coefficient α is given by:

$$\alpha = \frac{\left[\sum_{j=1}^{n} m_j \phi_j\right]^2}{\sum_{j=1}^{n} m_j \sum_{j=1}^{n} m_j \phi_j^2} \tag{5.17}$$

3. Plot capacity spectrum and 5% damped design spectrum together in ADRS format. Make initial estimate of performance point (defined as the point at which the capacity spectrum intersects a design spectrum whose damping has been artificially increased above 5% to account for the hysteretic damping in yielding elements). Normally the initial estimate is achieved by extending the linear part of the capacity spectrum until it intersects the 5% damped design spectrum.

4. Construct a bilinear approximation to the capacity spectrum using the same procedure as in FEMA 356 – see Figure 5.4 above. Define yield point coordinates as (a_y, d_y) and trial performance point coordinates as (a_{pi}, d_{pi}).

5. Calculate equivalent damping β_0 (% of critical) due to hysteresis:

$$\beta_0 = \frac{200(a_y d_{pi} - a_{pi} d_y)}{\pi a_{pi} d_{pi}} \tag{5.18}$$

6. Compute a new ADRS design spectrum taking account of this additional damping by applying the following spectral reduction factors SR_A and SR_V to the constant acceleration and constant velocity parts of the spectrum respectively:

$$SR_A = \frac{3.21 - 0.68\ln(\kappa\beta_0 + 5)}{2.12} \geq 0.33 \tag{5.19}$$

$$SR_V = \frac{2.31 - 0.41\ln(\kappa\beta_0 + 5)}{1.65} \geq 0.50 \tag{5.20}$$

where

$$\kappa = \begin{cases} 1.0 & \beta_0 \leq 16.25 \\ 1.13 - 0.008\beta_0 & \beta_0 > 16.25 \end{cases} \tag{5.21}$$

for structures exhibiting stable near-parallelogram hysteresis loops.

7. If new response spectrum intersects capacity spectrum at or sufficiently close to previous estimate of performance point, then the estimate is correct. Otherwise, re-estimate performance point and repeat from step 4.

8. Having converged to a performance point, convert the spectral displacement back to a target displacement d_t using Equation (5.16). Check member strengths and storey drifts are acceptable at this value of d_t.

5.3.5 Comments on application of the methods

The above methods were applied in a two-stage process. First, appropriate load patterns were developed and non-linear pushover analyses were performed in Sap. The failure point was identified (in the case of frames with dissipators this was usually when a dissipative link element reached its limiting deformation). The force-displacement data were then transferred to an Excel spreadsheet which performed the necessary computation of target displacement semi-automatically – a couple of parameters for the bilinear idealisation of the pushover curves had to be entered manually, allowing the analyst to retain some judgement.

On the whole this process was straightforward, but occasionally problems were encountered. In the capacity spectrum method, convergence difficulties sometimes occurred when the performance point lay close to the transition from the constant acceleration to the constant velocity part of the spectrum. In these cases, it was not always clear that a reliable solution had been obtained.

For the FEMA 356 method, a second problem which arose in the case of the dissipative frames was the bilinear idealisation. The raw pushover curves for these frames were approximately tri-linear in nature, with the first step change in gradient occurring as the first dissipators yielded, and a significant second step change taking place when hinges started to form in the beams. It is not obvious how best to reduce such a curve to bilinear form. Figure 5.5 illustrates a couple of sensible possibilities, depending on the location of the target displacement, which is, of course, not known at the outset of the process. Some iteration may therefore be necessary, and it may be difficult to get this to converge if the target displacement turns out to be close to the second gradient change (as is often the case). This problem does not arise with the EC8 method, where the bilinear idealisation is unique, if rather conservative.

For the modal pushover method, the first three modes were used in all cases except for the 3-storey frame, for which only two modes were used.

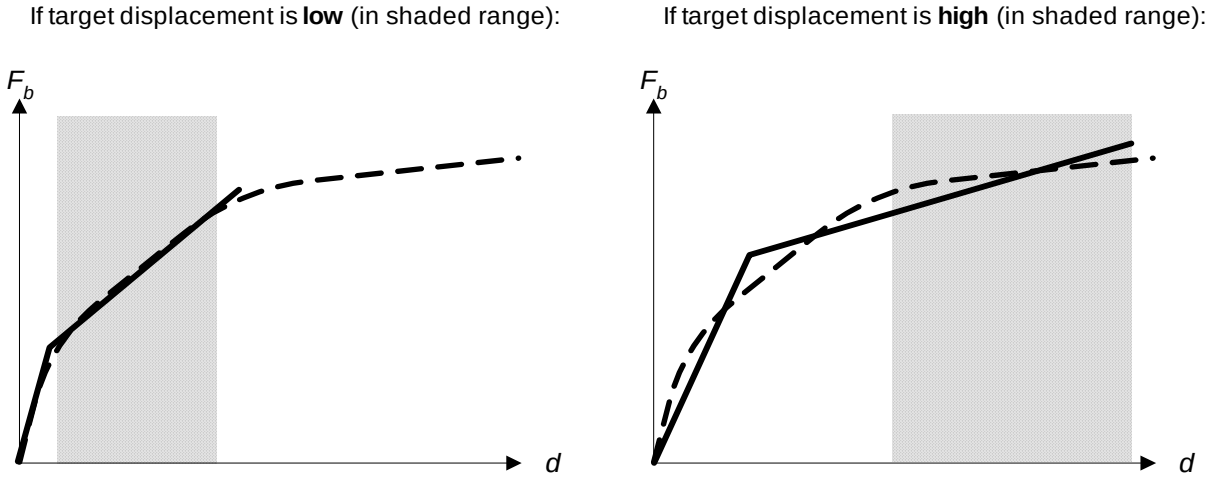

Figure 5.5 Possible bilinear idealisations of an approximately trilinear pushover curve

5.4 Simple Design Methods for Frames with Dissipators

The following methods were developed for preliminary design of frames with dissipators and used in the early stages of dissipator design, particularly by the UQ thesis group.

5.4.1 Iterative method based on linear static analysis

1. Perform elastic design of a moment-resisting frame with $q = 1$.

2. Make initial estimate of required dissipator capacities. e.g. Add diagonal braces to the MRF and re-analyse, then size dissipators at each level to yield at (say) 50% of the resulting brace forces. Plot hysteresis loops for the dissipators.

3. Perform a static analysis of the MRF under seismic loads. From the geometry of the deformed MRF, determine the extension of the brace/dissipator system. Assume all deformation takes place in the dissipator (i.e. that the brace is effectively rigid). Hence determine the dissipator force.

4. Adjust the seismic loads by subtracting the dissipator forces.

5. Repeat steps 3 and 4 until solution converges.

6. Adjust MRF member sizes to an appropriate level for the new forces.

7. Adjust dissipator sizes to give approximately uniform yielding up structure.

8. Repeat from step 3 until optimum solution is achieved.

5.4.2 Equivalent viscous damping method

1. Choose desired equivalent additional damping level to be supplied by dissipators, β_0 – say 15-20%.

2. Calculate corresponding spectral reduction factors using Equations (5.19) to (5.21). Hence determine equivalent static loads to be applied to structure. Apply these loads to a concentrically braced frame.

3. Choose dissipator characteristics: yield loads (< brace forces in step 2) and post-yield stiffnesses. Reanalyse structure with brace forces replaced by dissipator yield forces.

4. Use resulting nodal displacements to calculate the extensions of the brace/dissipator system and improved estimate of dissipator forces (= yield forces if elastic-perfectly plastic, greater if there is significant post-yield stiffness). Assume all deformation takes place in the dissipator (i.e. that the brace is effectively rigid).

5. Calculate energy absorbed in dissipators E_d and strain energy in remainder of structure E_s. Additional damping is then given by:

$$\beta_0 = \frac{E_d}{4\pi E_s} \tag{5.22}$$

6. Repeat from step 4 until damping approaches desired value and dissipator forces converge.

7. May then need to repeat from step 3 to ensure dissipators give reasonably uniform damping over height of building.

5.5 Time History Analysis

Non-linear time history analyses were used as a baseline case against which to compare the various non-linear static methods. Time history analysis was performed within Sap using the implicit integration method Hilber et al. (1977), in which the conventional equation of motion at a timestep is modified by the inclusion of a numerical damping parameter α, which takes a value between 0 and –1/3. With $\alpha = 0$ the method reduces to the well-known Newmark implicit scheme with $\beta = 1/4$ and $\gamma = 1/2$. When α takes a negative value it tends to dampen the higher modes of vibration, improving convergence at the cost of a small loss of accuracy. The analyses performed here used $\alpha = 0$ in all cases except for the friction-damped frames, which experienced some convergence problems due to the very small mass at the intersection of the link elements, which gave rise to some high frequency modes. For these analyses, therefore, a value of $\alpha = -0.05$ was used.

To give statistically significant results, each structure was subjected to thirty time history analyses, using the thirty spectrum-compatible earthquake records in Appendix A. The maximum, minimum, mean and standard deviation of each response parameter of interest was recorded.

6. Results

In this section results of the pushover and time history analyses are presented and discussed. Comparisons are made of estimated natural period, target displacement, base shear, plastic hinge formation, inter-storey drift and dissipative device deformation. Wherever possible, data from all analyses are presented in a single table, so that the reader can make comparisons both between different structural types and different analysis methods within a single table.

6.1 Natural period

Table 6.1 shows the natural periods of all buildings as determined by eigenvalue analysis and as estimated by the EC8 and FEMA 356 pushover methods. Looking first at the right-hand column, it can be seen the addition of bracing has the effect of roughly halving the initial natural period, implying a quadrupling of the structure's lateral stiffness. This period will, of course, be correct only at low displacement amplitudes, after which dissipator yield or slip will lead to some lengthening. It is also clear that the friction damped frames (FDFs) consistently have a slightly shorter period than the knee braced frames (KBFs), presumably due to the greater initial rigidity of the friction elements.

Storeys (R)		EC8		FEMA 356		Eigenvalue analysis
		Uni.	Mod.	Uni.	Mod.	
3	MRF	1.40	1.57	1.05	1.17	1.07
3	KBF	0.67	0.71	0.52	0.57	0.58
3	FDF	0.77	0.85	0.47	0.53	0.54
6	MRF	2.29	2.65	1.80	2.09	1.90
6	KBF	1.17	1.38	1.05	1.18	0.93
6	FDF	1.39	1.50	0.95	1.10	0.90
10(4.5)	MRF	2.43	2.87	2.04	2.39	2.4
10(1)	MRF	1.14	1.41	0.95	1.18	1.2
10	KBF	1.42	1.71	1.23	1.45	1.14
10	FDF	1.54	1.86	1.18	1.41	1.13

Key: *MRF = undamped moment resisting frame, KBF = knee braced frame, FDF = friction damped frame, Uni. = uniform load pattern, Mod. = modal load pattern*

Table 6.1 Natural periods (s) estimated by pushover methods compared with results of eigenvalue analysis

The comparison of the periods as estimated by pushover analysis with those determined by eigenvalue analysis is mainly a measure of the extent to which the bilinear idealisation of the pushover curve allow the initial elastic stiffness to be captured. Modest discrepancies here are not necessarily an indication of a flaw in the pushover method. Nevertheless, it is clear that the EC8 method, which assumes no post-yield stiffness (see Figure 5.3) generally tends to give a very low estimate of the initial stiffness, hence a high estimate of the period. The FEMA 356 method allows a much better fit to the actual pushover curve, and this is reflected in the similarity of the periods to those obtained by eigenvalue analysis.

Lastly, it is notable (if unsurprising) that uniform load patterns always produce a stiffer response, and so a lower estimate of the period, than modal loading patterns.

6.2 Target Displacements

Table 6.2 and Figures 6.1 – 6.3 show comparisons of the target displacements from the various pushover methods with the maximum roof displacements achieved in the time history analyses.

Looking first at the time history results in the right-hand three columns of Table 6.2 (quoted as the mean of the thirty analyses, and the mean ± one standard deviation), it is clear that both forms of retrofit are extremely effective in reducing the overall deformations of the frames, by a factor of more than 2. For the 10-storey frame, the dissipative frames deform less than the MRF designed to behave elastically. There is little difference and no consistent trend in the relative performances of the KBFs and FDFs.

St. (R)		EC8		FEMA 356		ATC 40		Modal push.	Time history analysis		
		Uni.	Mod.	Uni.	Mod.	Uni.	Mod.		–SD	Mean	+SD
3	MRF	296	331	221	248	221	247	249	186	206	227
3	KBF	139	148	104	118	88	133	118	77	87	97
3	FDF	163	179	96	109	166	186	110	76	89	102
6	MRF	428	428	385	428	368	427	434	272	333	395
6	KBF	251	295	223	252	230	265	254	132	143	154
6	FDF	297	321	204	235	279	307	239	123	141	160
10(4.5)	MRF	429	429	429	429	406	427	437	383	432	482
10(1)	MRF	257	318	214	266	214	266	270	259	286	312
10	KBF	298	360	258	305	248	284	310	185	199	212
10	FDF	324	391	249	297	268	336	302	142	163	184

Key: *MRF = undamped moment resisting frame, KBF = knee braced frame, FDF = friction damped frame, Uni. = uniform load pattern, Mod. = modal load pattern, –SD = (mean – standard deviation), +SD = (mean + standard deviation)*

Table 6.2 Target displacements (mm) estimated by pushover methods compared with maximum displacements in time history analysis

The performance of the various pushover methods is most easily assessed using Figures 6.1 – 6.3. Figure 6.1 shows the displacement estimates for the three ductile MRFs. All the pushover methods show reasonable agreement with the time-history results, generally within 1-2 standard deviations of the mean and nearly all erring on the conservative side, as is desirable for an approximate design method. The most notable exception is that the EC8 approach gives rather over-conservative results in the case of the 3-storey frame. For the 10-storey frame, all the methods give very similar estimates, very close to the mean of the time history results. For this case, the ATC 40 capacity spectrum method gives slightly unconservative results. The good performance for this structure is to be expected, since its period exceeds 2 seconds, corresponding to the constant displacement part of the EC8 response spectrum, Figure 3.1.

Turning to the dissipative frames (see Figure 6.2 for KBFs, Figure 6.3 for FDFs), note that the standard deviations of the time-history analyses are much lower than for the MRFs. This is to be expected as, with the exception of the dissipative elements, the structures are responding nearly elastically. Clearly all the pushover methods tend to err rather heavily on the conservative side, particularly for the taller structures. The FEMA 356 method is probably the most realistic, though even this gives results several standard deviations above the mean in some cases. This would seem to imply that, while pushover analysis models non-linearity in all the elements, it does not take sufficient account of the energy dissipation provided by elements which are undergoing large non-linear cycles from a very early stage in the earthquake. This calls into question the appropriateness of pushover analysis for frames with dissipators.

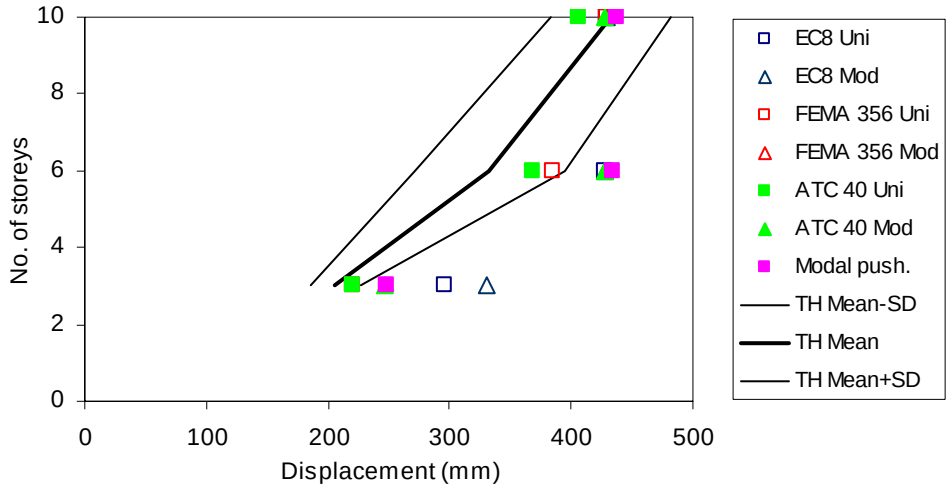

Figure 6.1 Comparison of target displacements with time history results for ductile moment-resisting frames

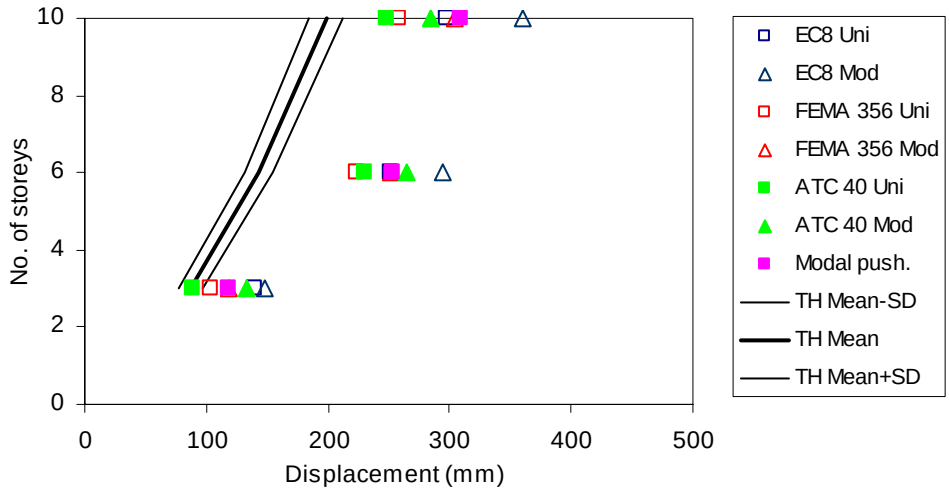

Figure 6.2 Comparison of target displacements with time history results for knee braced frames

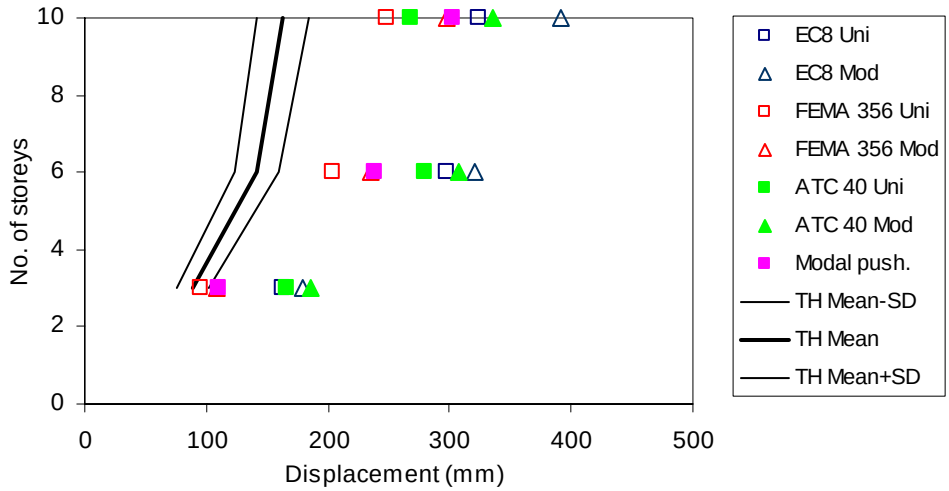

Figure 6.3 Comparison of target displacements with time history results for friction damped frames

6.3 Base Shear

Table 6.3 and Figures 6.4 – 6.6 show comparisons of base shears from the various pushover methods with the maximum values achieved in the time history analyses, following the same format as for target displacements above.

On the basis of the time history results, it is noticeable that the addition of knee bracing slightly increases the base shear carried by the structure, whereas the addition of friction dampers results in a modest reduction in base shear. There are two interacting effects in play here – the increased stiffness provided by the bracing shifts the natural period of the structure towards the peak of the response spectrum, thus increasing the loads it must carry, while the energy dissipation tends to reduce the loads. In the case of the friction dampers, the very low post-slip stiffness proves better at limiting the loads attracted by the structure than the rather higher post-yield stiffness of the hysteretic elements. However, looking at the 10-storey frames, both dissipative designs result in less than half of the base shear of the elastic design, resulting a much more economic structure.

For the ductile MRFs, Figure 6.4 shows that the pushover methods give rather low forces for the 3-storey frame but good estimates for the taller frames. For the dissipative frames, Figures 6.5 and 6.6, the methods appear to give reasonable estimates for the 3-storey frame but rather high estimates for the taller frames. This is particularly true of the EC8 approach. The ATC 40 method gives unconservative results for the case of the 3-storey frame.

These results are broadly consistent with those for target displacement discussed above, with the exception of the low base shear estimates in the 3-storey frames, the reason for which is not obvious.

Lastly, note that an increasing trend of base shear with height is not expected here, because the 3- and 6-storey frames carry considerably more load per floor than the 10-storey frame.

St. (R)		EC8		FEMA 356		ATC 40		Modal push.	Time history analysis		
		Uni.	Mod.	Uni.	Mod.	Uni.	Mod.		–SD	Mean	+SD
3	MRF	2340	1971	2185	1881	2185	1879	2177	2320	2448	2552
3	KBF	3863	3430	3668	3213	3405	3333	3302	3006	3196	3401
3	FDF	2881	2537	2443	2110	2890	2553	2302	2102	2240	2433
6	MRF	2747	2173	2692	2173	2666	2173	2583	2650	2815	2979
6	KBF	4459	3784	4380	3665	4398	3703	4121	2929	3155	3382
6	FDF	3426	2770	3132	2565	3397	2744	2889	1993	2175	2357
10(4.5)	MRF	1717	1358	1717	1358	1685	1355	1600	1518	1613	1708
10(1)	MRF	5136	3877	4311	3383	4311	3383	3694	3746	4167	4587
10	KBF	2837	2387	2647	2214	2589	2131	2496	1675	1802	1928
10	FDF	2273	1897	2021	1673	2101	1786	1921	1240	1323	1405

Key: *MRF = undamped moment resisting frame, KBF = knee braced frame, FDF = friction damped frame, Uni. = uniform load pattern, Mod. = modal load pattern, –SD = (mean – standard deviation), +SD = (mean + standard deviation)*

Table 6.3 Base shears (kN) estimated by pushover methods compared with maximum base shears in time history analysis

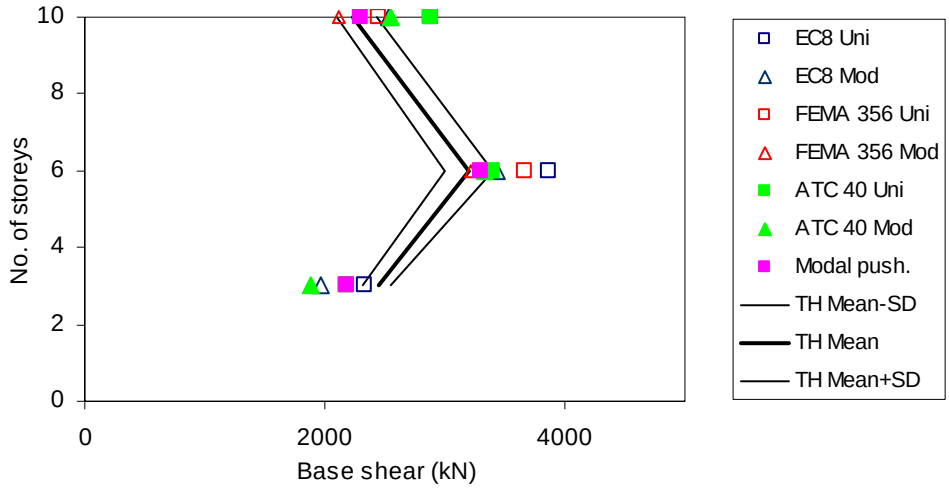

Figure 6.4 Comparison of base shears with time history results for ductile moment-resisting frames

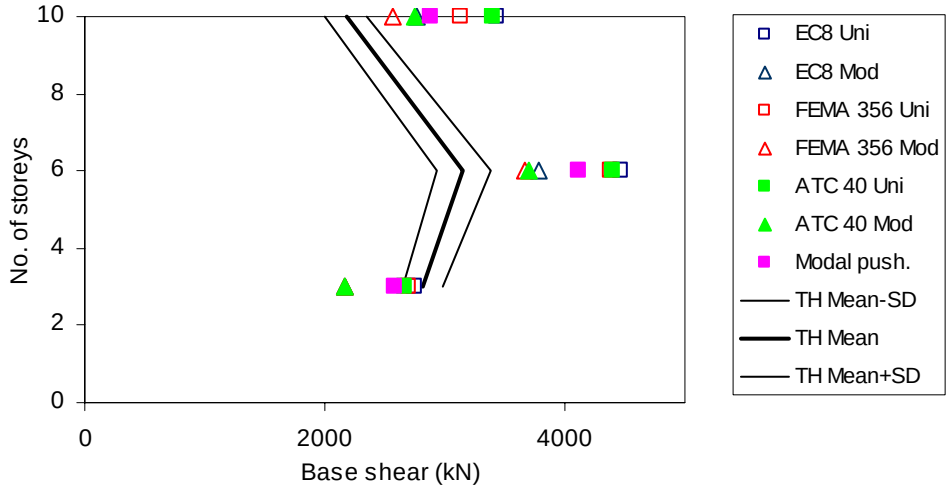

Figure 6.5 Comparison of base shears with time history results for knee braced frames

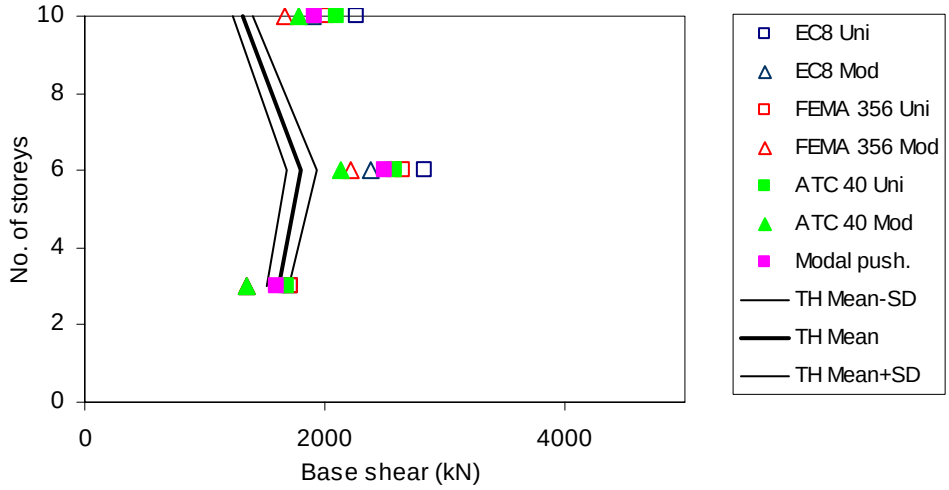

Figure 6.6 Comparison of base shears with time history results for friction damped frames

6.4 Plastic Hinge Formation

Table 6.4 shows the number of plastic hinges formed in each structure under the design earthquake, compared to the minimum, mean and maximum values from the time history analyses.

Again these results are quite consistent with those for target displacement. For the MRFs the estimates of plastic hinge formation produced by the pushover methods agree quite well with the time history results, with the exception of the 10-storey ductile frame, where the number of hinges is underestimated. For the dissipative frames, the pushover methods all seem to underestimate the degree of improvement achieved.

St. (R)		EC8		FEMA 356		ATC 40		Time history analysis		
		Uni.	Mod.	Uni.	Mod.	Uni.	Mod.	Min	Mean	Max
3	MRF	20	22	16	20	13	15	15	18.9	22
3	KBF	12	12	7	7	2	10	0	1.4	6
3	FDF	13	16	3	6	13	16	0	1.9	6
6	MRF	31	27	28	27	26	27	26	33.5	40
6	KBF	19	22	18	19	19	21	0	0.5	3
6	FDF	24	26	10	13	24	25	0	0.7	8
10(4.5)	MRF	29	33	29	33	27	33	24	39.2	53
10(1)	MRF	7	13	0	8	0	8	10	12.0	14
10	KBF	16	23	7	11	6	6	0	1.3	3
10	FDF	18	29	5	6	6	18	0	0	0

Key: *MRF = undamped moment resisting frame, KBF = knee braced frame, FDF = friction damped frame, Uni. = uniform load pattern, Mod. = modal load pattern, –SD = (mean – standard deviation), +SD = (mean + standard deviation)*

Table 6.4 Numbers of plastic hinges formed in main frame elements as determined by pushover methods and time history analysis

6.5 Inter-Storey Drifts

Drift profiles estimated by the various pushover methods for the ten structures studied are compared to time history results in Figures 6.7 – 6.16. In many cases the drifts are over-estimated by the approximate methods, in line with the overestimate of target displacement presented earlier.

Of more interest are the shapes of the drift profiles, where the superiority of the modal pushover approach can be clearly seen. In terms of drift profile, all the methods show reasonable agreement with the time history results for the 3-storey frames (Figures 6.7 – 6.9). For the 6- and 10-storey frames (Figures 6-10 – 6.16), however, there is a consistent tendency in the EC8, FEMA 356 and ATC 40 methods to overestimate drifts in the lower storeys and underestimate them at the top. This error is largely eliminated in all cases by using the modal pushover approach (an SRSS combination of the drifts obtained using load patterns corresponding to the first three mode shapes). The only exception to this is the 10-storey elastic frame, where all methods produce reasonable profiles, though even here the modal pushover method gives arguably better results.

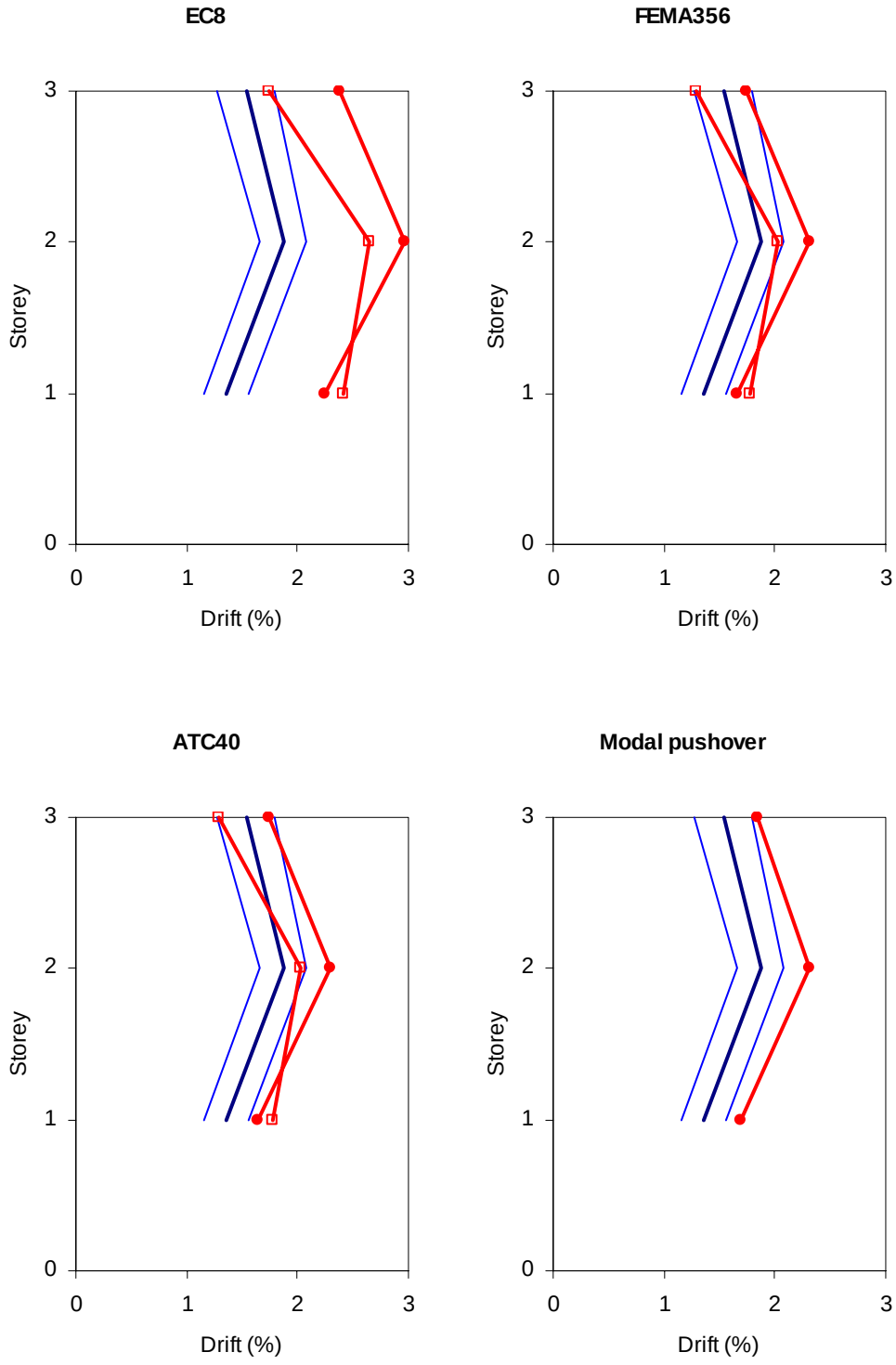

Key: *Blue lines: Time history mean and mean ± one standard deviation*
Red squares: pushover results using uniform load pattern
Red circles: pushover results using modal load pattern

Figure 6.7 Inter-storey drift comparisons for 3-storey ductile MRF

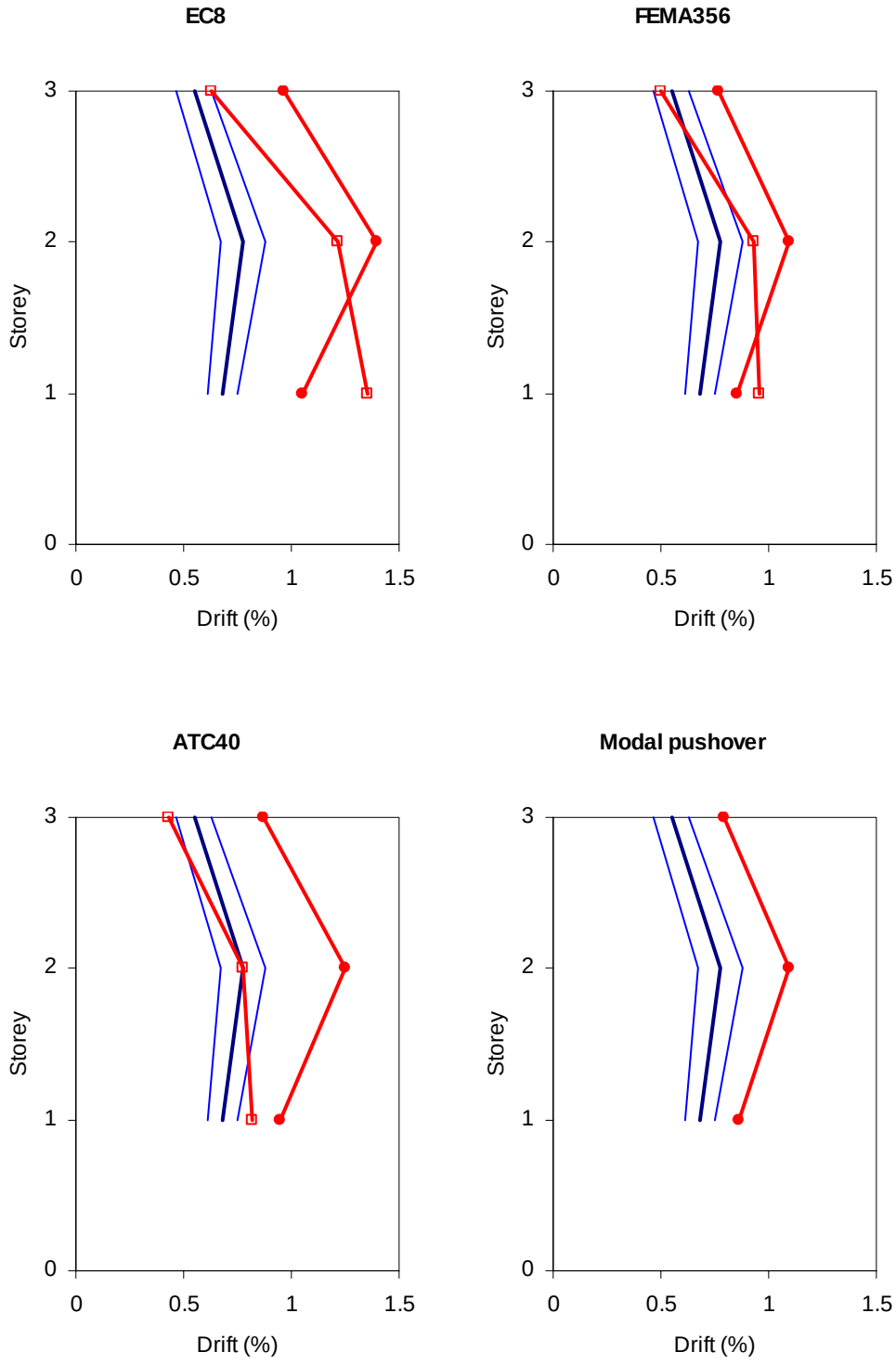

Key: *Blue lines: Time history mean and mean ± one standard deviation*
Red squares: pushover results using uniform load pattern
Red circles: pushover results using modal load pattern

Figure 6.8 Inter-storey drift comparisons for 3-storey knee braced frame

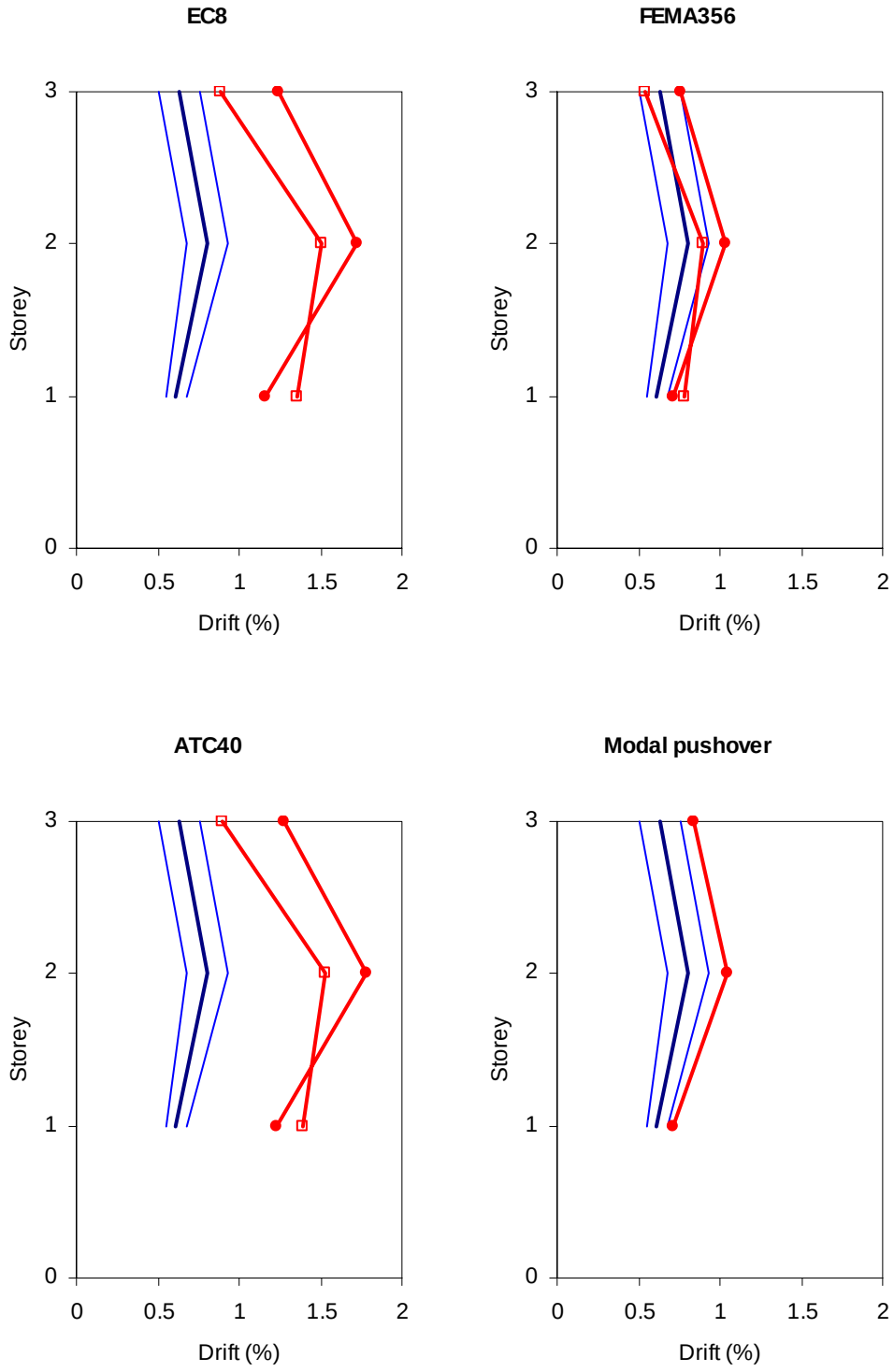

Key: *Blue lines: Time history mean and mean ± one standard deviation*
Red squares: pushover results using uniform load pattern
Red circles: pushover results using modal load pattern

Figure 6.9 Inter-storey drift comparisons for 3-storey friction damped frame

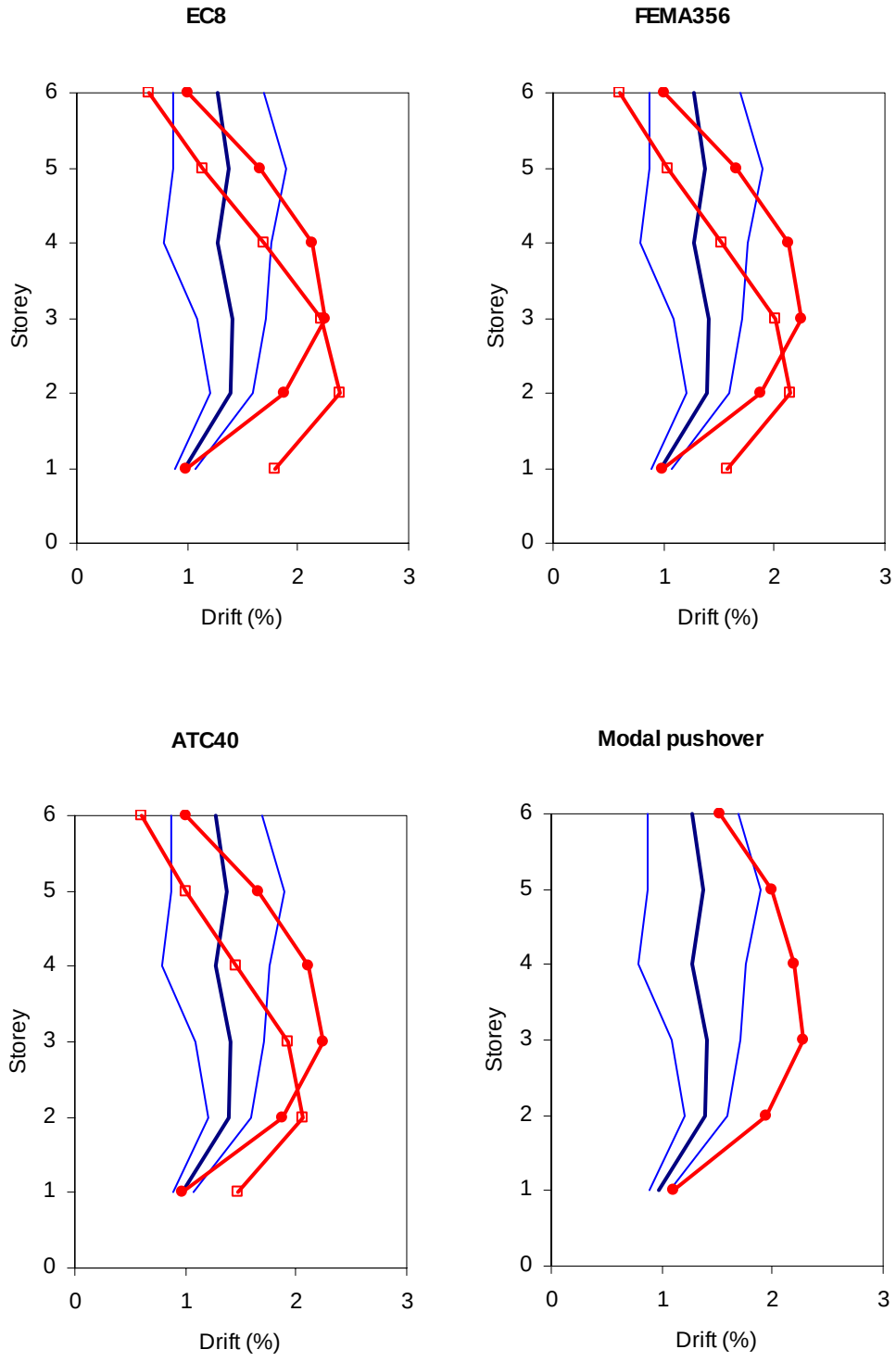

Key: *Blue lines: Time history mean and mean ± one standard deviation*
Red squares: pushover results using uniform load pattern
Red circles: pushover results using modal load pattern

Figure 6.10 Inter-storey drift comparisons for 6-storey ductile MRF

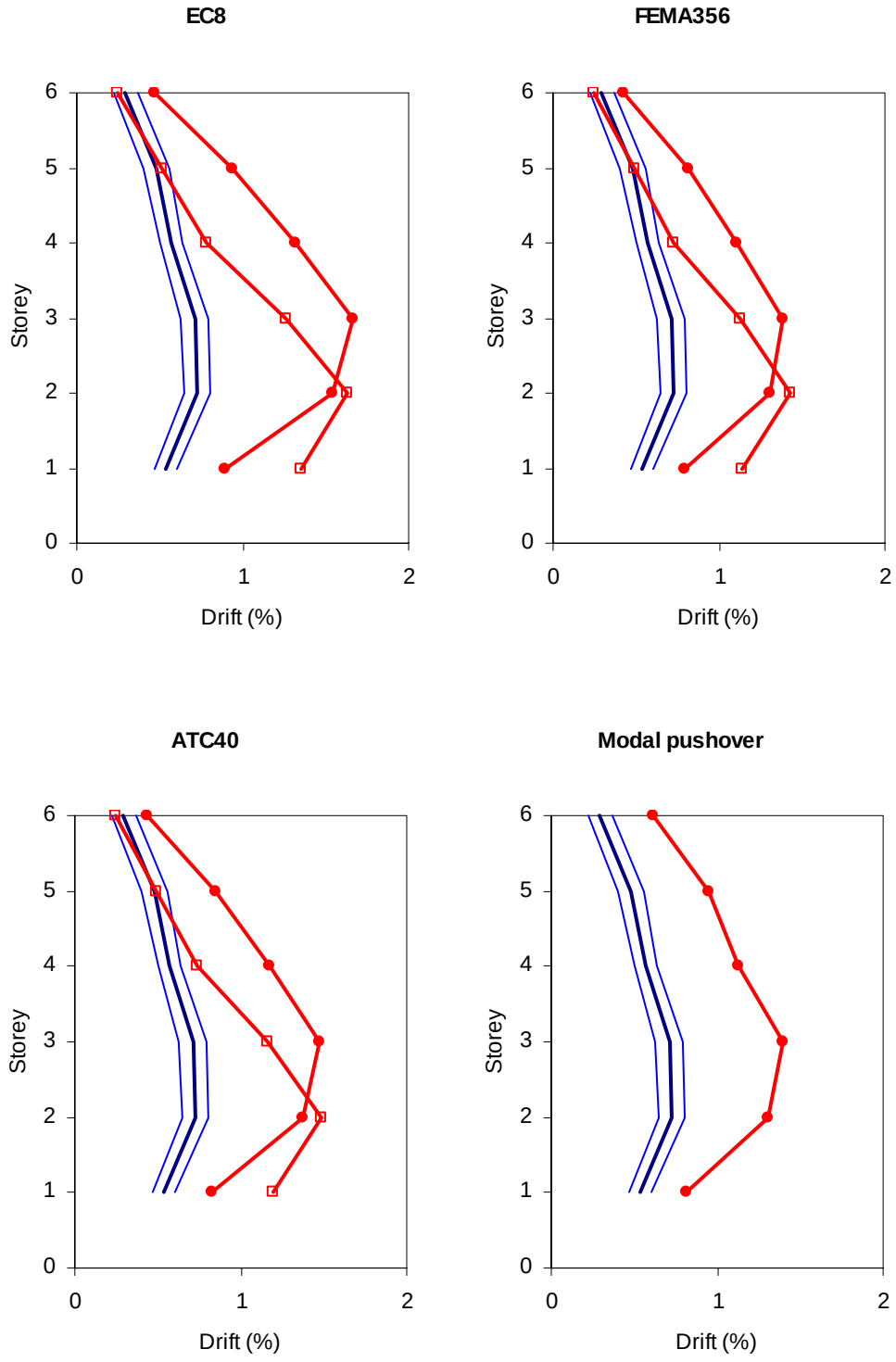

Key: *Blue lines: Time history mean and mean ± one standard deviation*
Red squares: pushover results using uniform load pattern
Red circles: pushover results using modal load pattern

Figure 6.11 Inter-storey drift comparisons for 6-storey knee braced frame

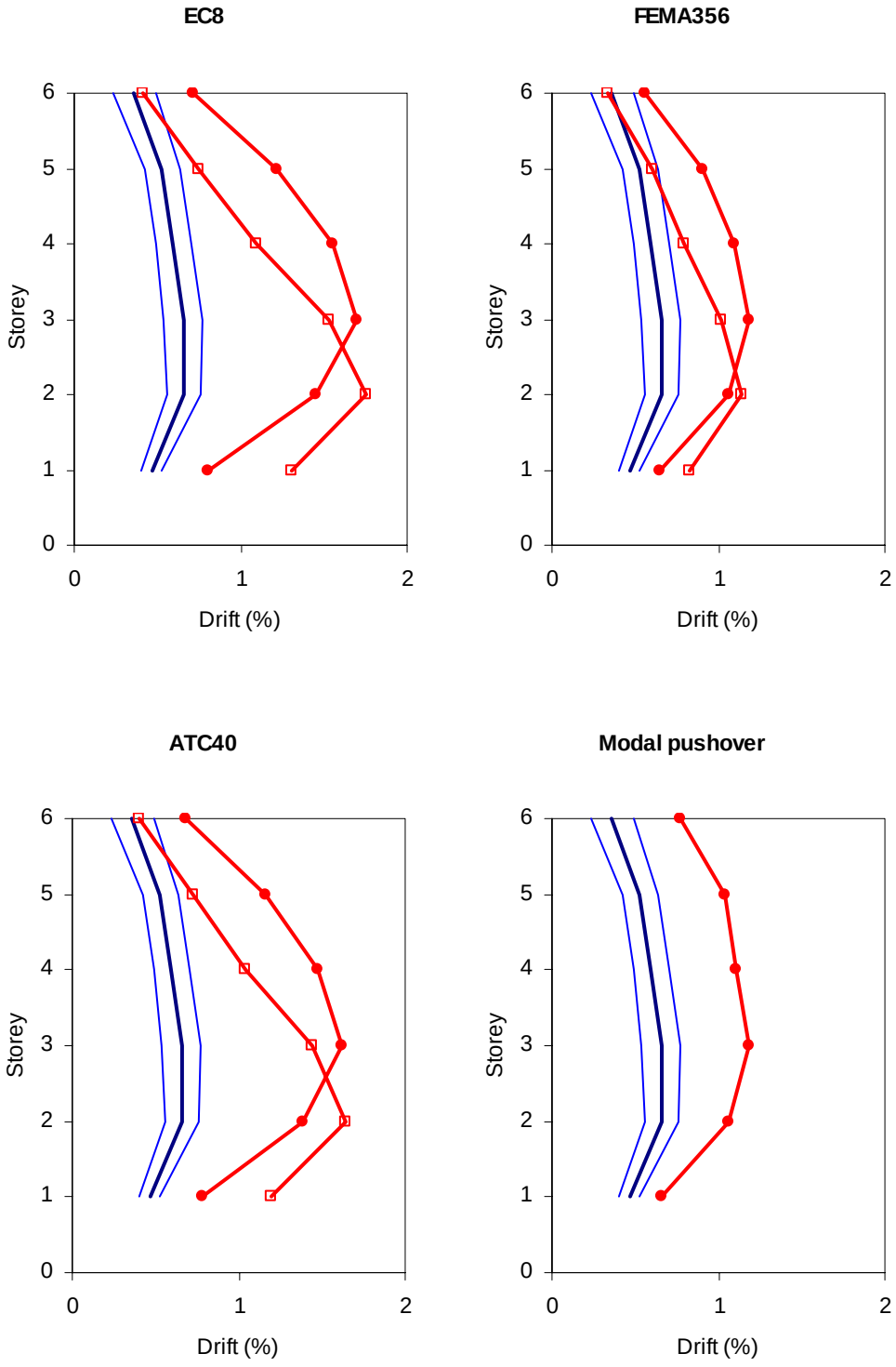

Key: *Blue lines: Time history mean and mean ± one standard deviation*
Red squares: pushover results using uniform load pattern
Red circles: pushover results using modal load pattern

Figure 6.12 Inter-storey drift comparisons for 6-storey friction damped frame

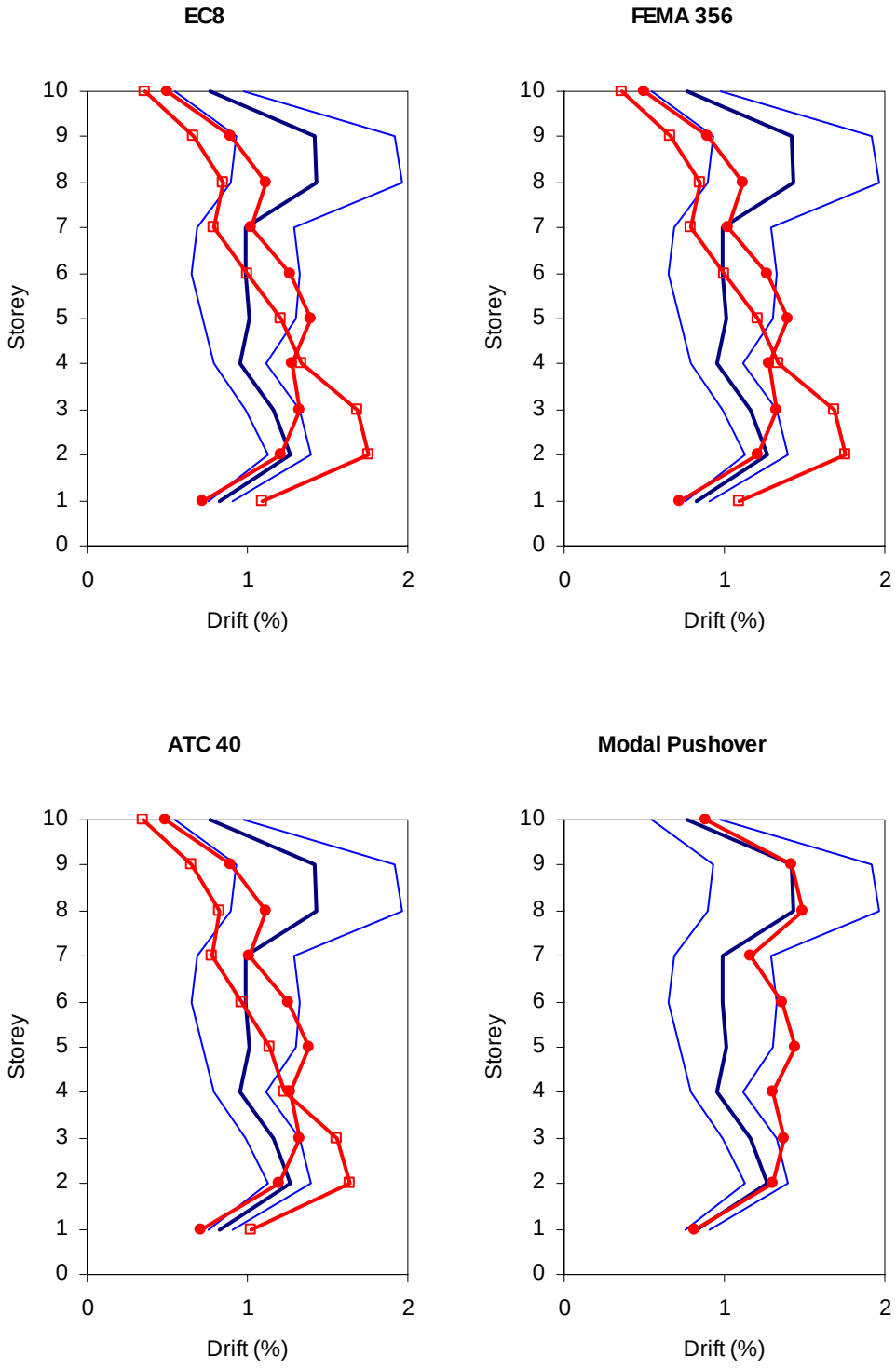

Key: *Blue lines: Time history mean and mean ± one standard deviation*
Red squares: pushover results using uniform load pattern
Red circles: pushover results using modal load pattern

Figure 6.13 Inter-storey drift comparisons for 10-storey ductile MRF (R = 4.5)

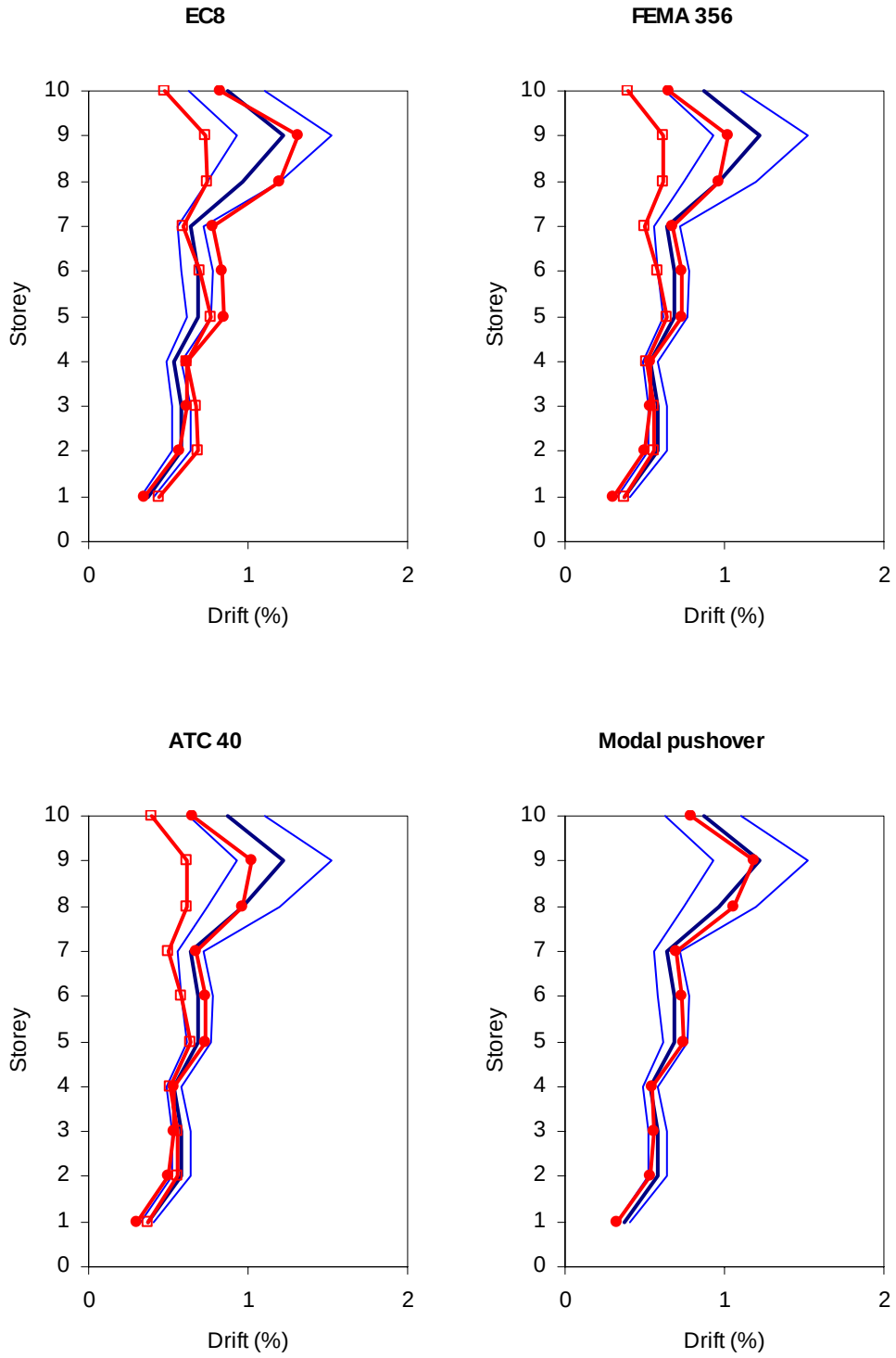

Key: *Blue lines: Time history mean and mean ± one standard deviation*
Red squares: pushover results using uniform load pattern
Red circles: pushover results using modal load pattern

Figure 6.14 Inter-storey drift comparisons for 10-storey elastic MRF (R = 1)

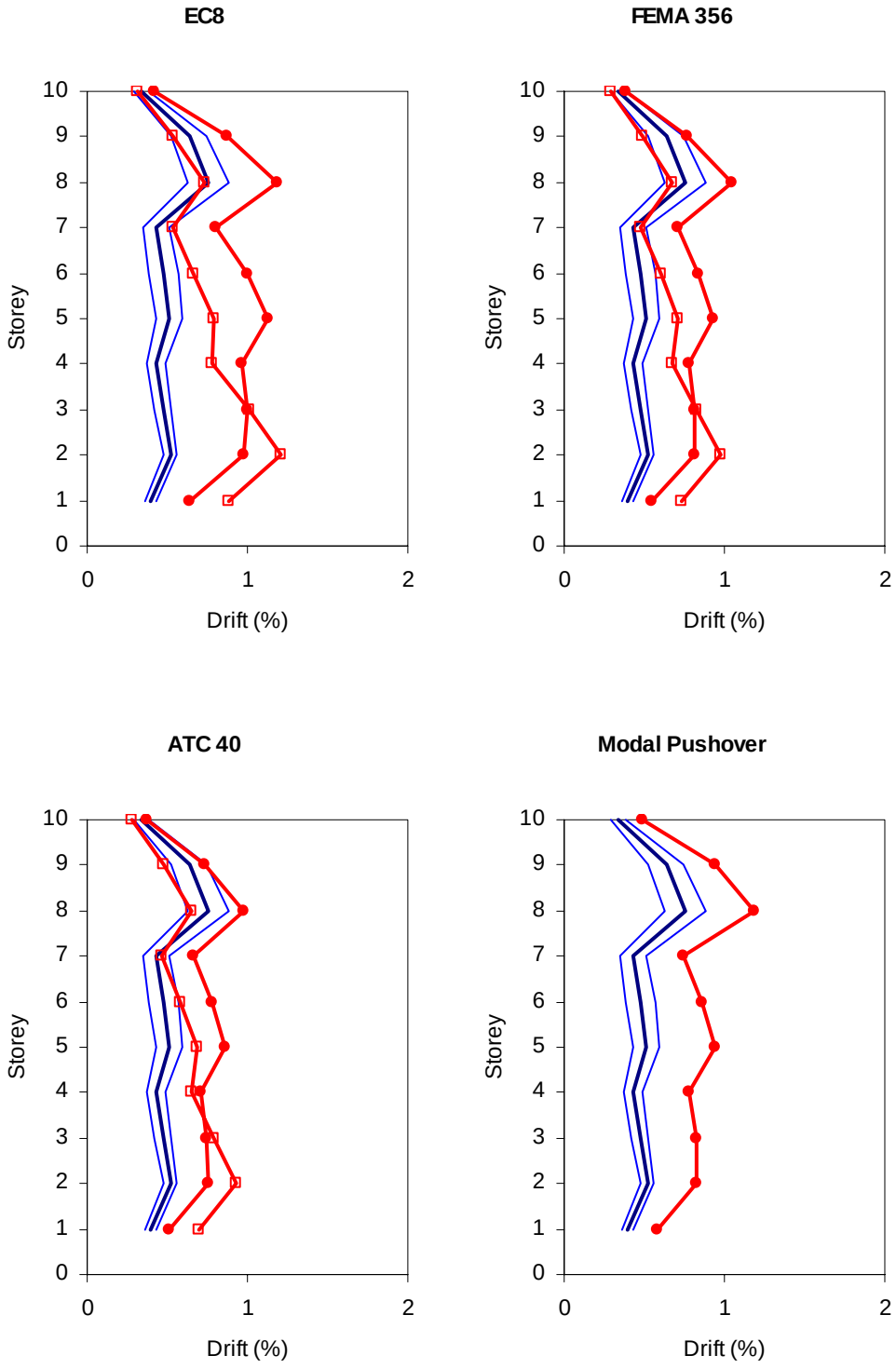

Key: *Blue lines: Time history mean and mean ± one standard deviation*
Red squares: pushover results using uniform load pattern
Red circles: pushover results using modal load pattern

Figure 6.15 Inter-storey drift comparisons for 10-storey knee braced frame

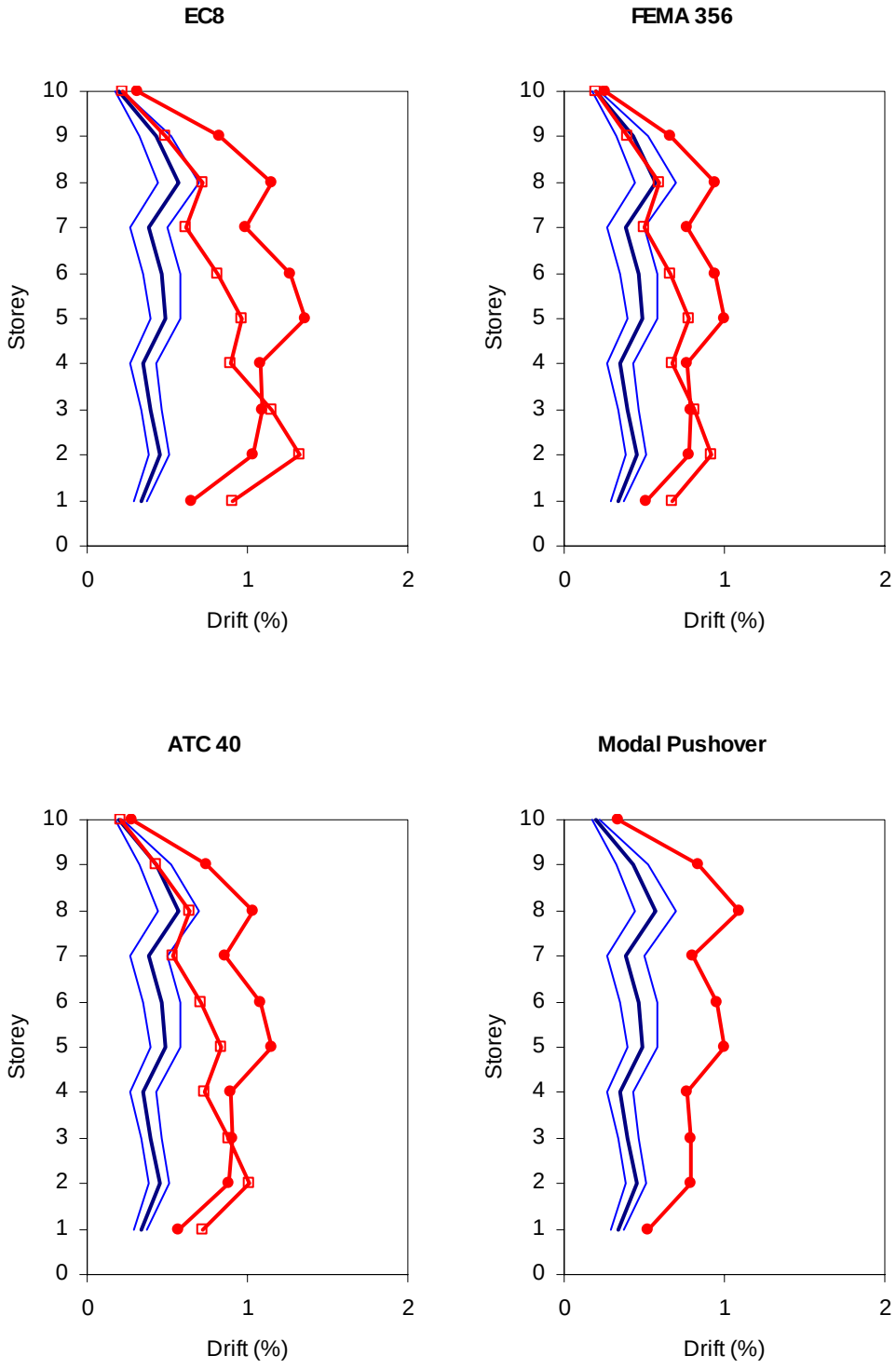

Key: *Blue lines: Time history mean and mean ± one standard deviation*
Red squares: pushover results using uniform load pattern
Red circles: pushover results using modal load pattern

Figure 6.16 Inter-storey drift comparisons for 10-storey friction damped frame

6.6 Link Deformations

Table 6.5 shows some summary statistics on link element deformations during the time history analyses. For the 3- and 6-storey frames, all dissipative elements were deformed into the non-linear range under the action of each of the thirty earthquakes. For the 10-storey frames, a very small number (generally one or two) of the dissipative elements remained in their elastic range in some of the earthquakes, suggesting that some further refinement of the dissipator design would be possible. All dissipators stayed comfortably below their ultimate deformations in all cases.

Storeys		u_y	u_{ult}	Max. deformations in TH analysis		
				Min.	Mean	Max.
3	KBF	5	40	15.0	20.2	30.5
6	KBF	5	40	7.7	17.0	27.5
10	KBF	4	40	3.8	10.2	21.6
3	FDF	2	30	9.3	13.9	22.8
6	FDF	2	30	6.9	11.6	18.2
10	FDF	1.6	30	1.3	6.4	11.7

Key: *KBF = knee braced frame, FDF = friction damped frame, u_y = yield or slip deformation of dissipator/brace link element, u_{ult} = failure deformation of link element*

Table 6.5 Link element deformations (mm) in time history analyses

7. Conclusions

1. An extensive analysis and design study of 3-, 6- and 10-storey frames, both undamped MRFs and retrofitted with hysteretic and frictional dissipators has been performed. Frames were modelled using the finite element program Sap2000 and were analysed using both non-linear static pushover analysis and non-linear time history analysis under an ensemble of thirty spectrum-compatible accelerograms. The results have been used to assess the accuracy and usability of several pushover design approaches.

2. It was found that both dissipative systems led to substantial improvements in frame performance, specifically (on the basis of the time history results):

   a) The retrofits succeeded in their principle aim of virtually eliminating plastic hinge formation in the main frame elements, with all the retrofitted frames developing few or no hinges under most of the thirty earthquake records.

   b) Roof displacements and inter-storey drifts were reduced by a factor of more than 2 by both systems, with the frictional system giving slightly greater reductions. For a 10-storey frame, the reduction in displacements was significantly greater than was achieved by redesigning the MRF to respond nearly elastically.

   c) Base shears were of a similar order of magnitude to those for the undamped frames – slightly larger for the hysteretically damped frames, lower for the friction damped

frames. For the 10-storey frame, this is in contrast to the performance of an elastically designed MRF, which gave a base shear of more than twice that of the ductile MRF.

3. Pushover analyses were found to be a useful design tool for the unretrofitted frames, giving good estimates of the overall displacement demands, base shears and plastic hinge formation. However, the EC8 procedure gave rather conservative results for the 3-storey frame.

4. The various pushover approaches proved less successful at estimating the performance of the dissipative frames, where they appeared to underestimate the beneficial effects of energy dissipation. Specifically:

   a) Target displacements were significantly overestimated, especially for the taller (longer period) frames.

   b) Base shears were overestimated by a rather smaller margin for the 6- and 10-storey frames but underestimated by some methods for the 3-storey frames.

   c) Plastic hinge formation in the main frame elements was greatly overestimated in comparison with the results of time history analysis.

   d) For the FEMA 356 and ATC 40 methods, it is necessary to fit a bilinear idealisation to what is in many cases an essentially tri-linear curve. This can be difficult to do unambiguously.

5. Of the various pushover methods assessed, the FEMA 356 approach appears to offer the most accurate and realistic estimate of seismic performance, with the exception of drift distribution (see point 6. below).

6. For the 6- and 10-storey frames (both ductile MRFs and dissipative frames), pushover methods using load patterns based on a uniform or first-mode force distribution gave rather poor estimates of the distribution of inter-storey drift with height. Far better drift estimates were obtained using the modal pushover method, in which pushover results obtained using force distributions based on the first three modes are combined by the SRSS method.

References

Aiken I.D., Kelly J.M. (1992) Comparative study of four passive energy dissipation systems. *Bulletin of New Zealand Society of Earthquake Engineering*, **25**(3), 175-192.

Aristazabal-Ochoa J.D. (1986) Disposable knee bracing: improvement in seismic design of steel frames. *J. Struct. Engng, Amer. Soc. Civ. Engrs*, **112**, 1544-1553.

AS 1170.4 (1993) *Minimum design loads on structures. Part 4: Earthquake loads*. Australian Standard, Homebush NSW.

ATC 40 (1996) Seismic evaluation and retrofit of concrete buildings. *Report ATC40,* Applied Technology Council, Redwood City CA.

Chintanapakdee C., Chopra A.K. (2003) Evaluation of modal pushover analysis using generic frames. *Earthquake Engng Struct. Dyn.*, **32**, 417-442.

Chopra A.K., Goel R.K. (2002) A modal pushover analysis procedure for estimating seismic demands for buildings. *Earthquake Engng Struct. Dyn.*, **31**, 561-582.

Constantinou M.C., Soong T.T., Dargush G.F. (1998) Passive energy dissipation systems for structural design and retrofit. *MCEER Monograph No. 1*, Multidisciplinary Center for Earthquake Engineering Research, Buffalo.

CSI (2002) *Sap2000, Version 8: Integrated software for structural analysis and design.* Computers and Structures Inc., Berkeley CA.

EC8 (2003) *Eurocode 8: Design of structures for earthquake resistance. General rules, seismic actions and rules for buildings*. EN1998-1:2003, British Standards Institution, London.

Fajfar P., Fischinger M. (1988) N2 – a method for non-linear seismic analysis of regular structures. *Proc. 9th World Conf. on Earthquake Engineering*, Tokyo/Kyoto, Vol. 5, 111-116.

FEMA 356 (2000) Prestandard and commentary for the seismic rehabilitation of buildings. *Report FEMA 356*, Federal Emergency Management Agency, Washington DC.

Filiatrault A., Cherry S. (1987) Performance evaluation of friction damped braced frames under simulated earthquake loads. *Earthquake Spectra*, **3**(1), 57-78.

Gasparini D.A., Vanmarcke E.H. (1976) Simulated earthquake motions compatible with prescribed response spectra. *Research Report R76-4*, Department of Civil Engineering, Massachusetts Institute of Technology, Cambridge, Massachusetts.

Hilber H.M., Hughes T.J.R., Taylor R.L. (1977) Improved numerical dissipation for time integration in structural dynamics. *Earthquake Engng Struct. Dyn.*, **5**, 283-292.

Krawinkler H., Seneviratna G. (1998) Pros and cons of a pushover analysis for seismic performance evaluation. *Eng. Struct.*, **20**, 452-464.

Lawson R.S., Vance V., Krawinkler H. (1994) Nonlinear static pushover analysis – why, when and how? *Proc. 5th US Conf. on Earthquake Engineering*, Chicago IL, Vol. 1, 283-292.

NEHRP (1997) Recommended provisions for seismic regulations for new buildings and other structures. *Report FEMA 302*, Federal Emergency Management Agency, Washington DC.

Pall A.S., Marsh C. (1982) Response of friction damped braced frames. *J. Struct. Engng, Amer. Soc. Civ. Engrs*, **108**(6), 1313-1323.

Ramirez O.M., Constantinou M.C., Kircher C.A., Whittaker A.S., Johnson M.W., Gomez J.D., Chrysostomou C.Z. (2001) Development and evaluation of simplified procedures for analysis and design of buildings with passive energy dissipation systems. *Technical Report MCEER-00-0010*, Multidisciplinary Center for Earthquake Engineering Research, Buffalo NY.

Soong T.T., Spencer B.F. (2002) Supplemental energy dissipation: state-of-the-art and state-of-the-practice. *Engineering Structures*, **24**, 243-259.

Williams M.S., Albermani F. (2003) Monotonic and cyclic tests on shear diaphragm dissipators for steel frames. *Civil Engineering Research Bulletin No. 23*, Department of Civil Engineering, University of Queensland, Brisbane.

Williams M.S., Blakeborough A., Clement D., Bourahla N. (2002) Seismic behaviour of knee braced frames. *Proc. Instn Civ. Engrs: Structs & Bldgs*, **152**, 147-155.

Wu B., Zhang J., Williams M.S. (2003) Behavior of Pall-typed frictional dampers. Submitted to *J. Engng Mech., Amer. Soc. Civ. Engrs*.

Xu T.L., Zhang W.S. (2001) Modal analysis and seismic response of steel frames with connection dampers. *Engineering Structures*, **23**, 385-396.

Appendix A. Spectrum-Compatible Time Histories

Thirty time histories were generated using the program Simqke (Gasparini and Vanmarcke, 1976), which generates statistically independent accelerograms based on a user-specified duration envelope and velocity response spectrum.

The envelope adopted had a rise time of 2 seconds, a strong motion duration of 10 seconds and a decay time of 8 seconds. The spectrum adopted was the Eurocode 8 (2003) Type 1 spectrum (for moderate or large events), soil type C (dense sand or gravel, or stiff clay). After generating an initial thirty accelerograms, the corresponding spectra were computed and the degree to which they matched the target spectrum was assessed by eye. On this basis, several of the time histories were rejected and replaced by new ones until an acceptable fit was achieved.

The following pages show the thirty time histories and the degree to which they fit the specified duration envelope and response spectrum (plotted in terms of both acceleration and velocity). The agreement is generally within about 10% of the target near the peak of the acceleration spectrum, and much better than that over most of the range of interest. Occasionally there are slightly larger discrepancies at longer periods, and these are particularly obvious when plotted in terms of velocity.

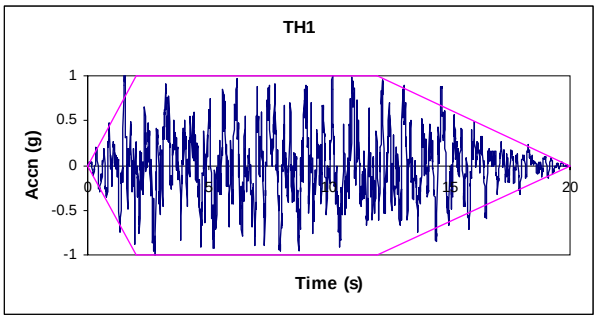
TH1
Accn (g)
Time (s)

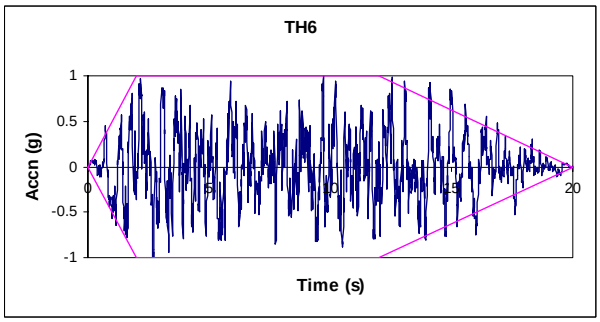
TH6
Accn (g)
Time (s)

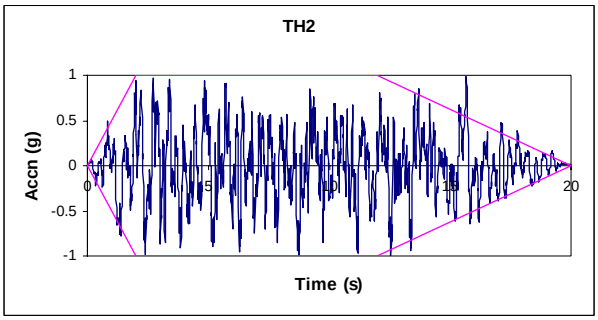
TH2
Accn (g)
Time (s)

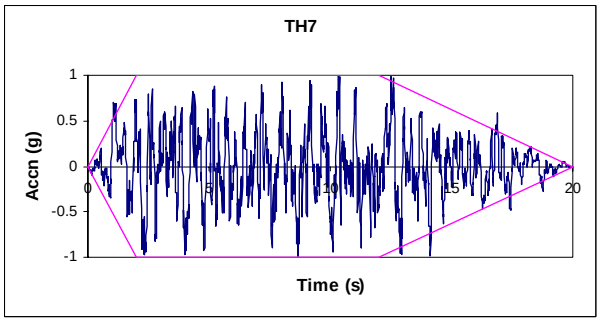
TH7
Accn (g)
Time (s)

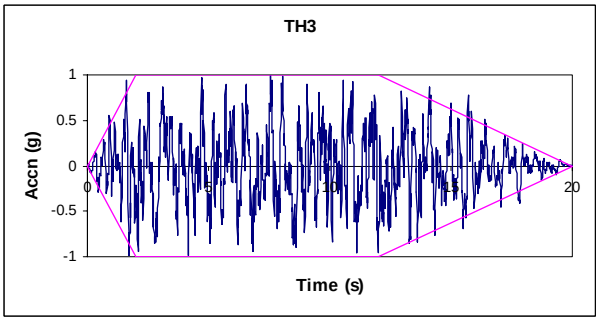
TH3
Accn (g)
Time (s)

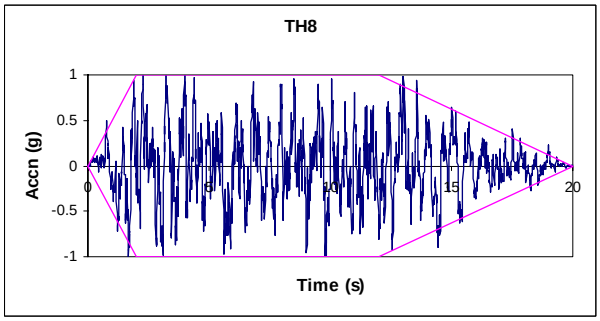
TH8
Accn (g)
Time (s)

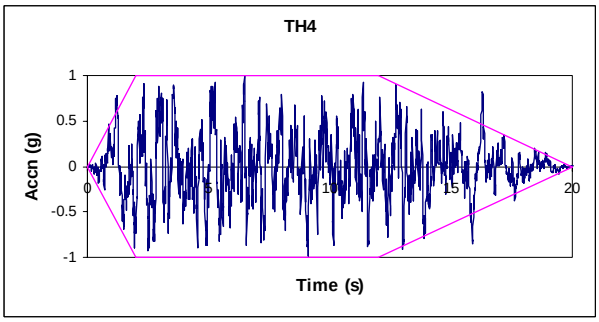
TH4
Accn (g)
Time (s)

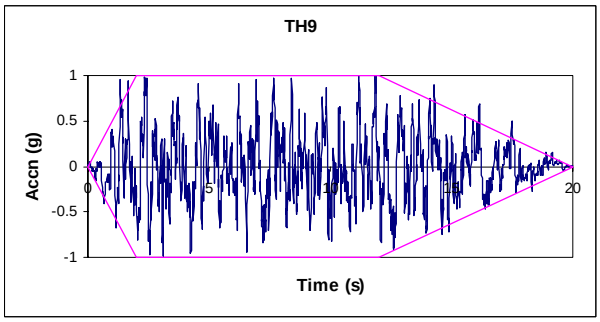
TH9
Accn (g)
Time (s)

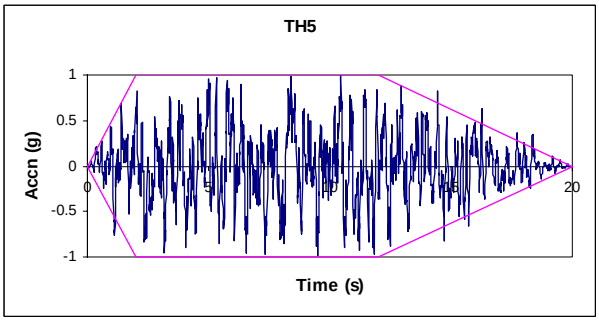
TH5
Accn (g)
Time (s)

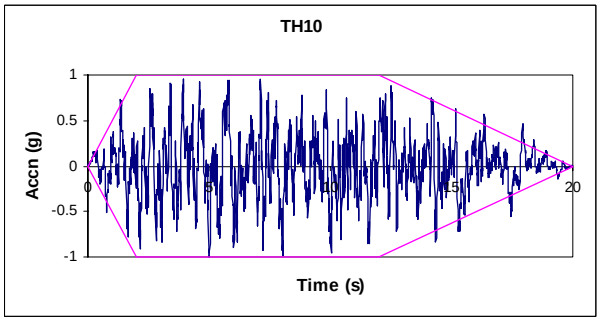
TH10
Accn (g)
Time (s)

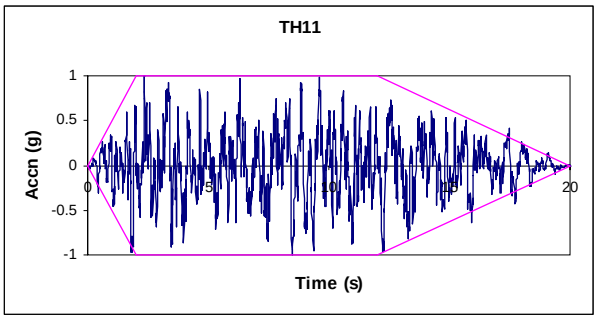
TH11
Accn (g)
Time (s)

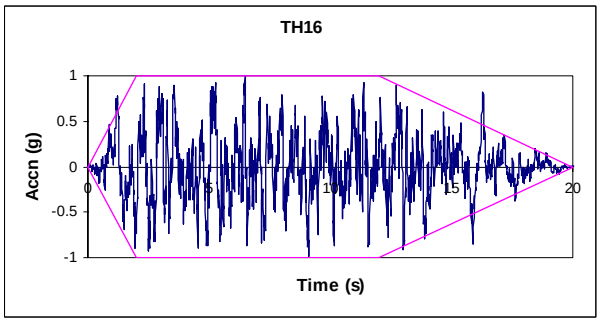
TH16
Accn (g)
Time (s)

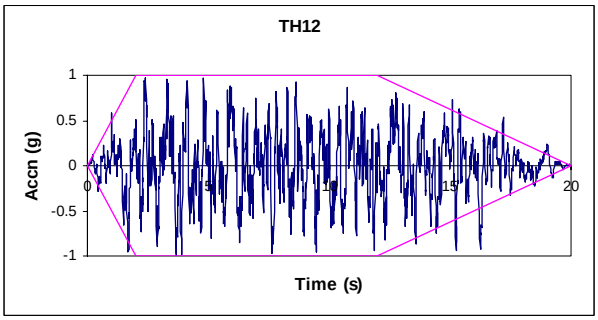
TH12
Accn (g)
Time (s)

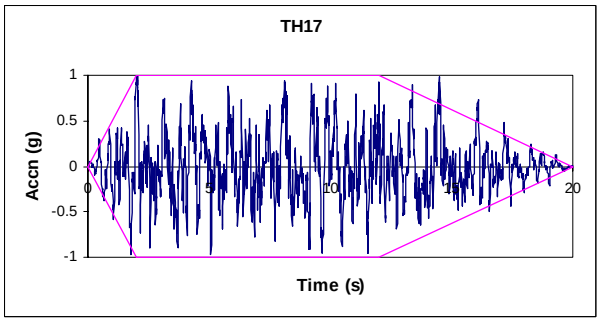
TH17
Accn (g)
Time (s)

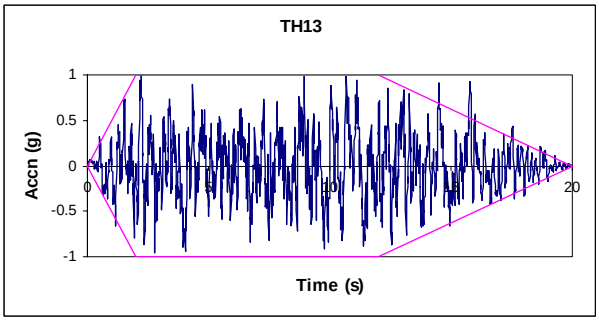
TH13
Accn (g)
Time (s)

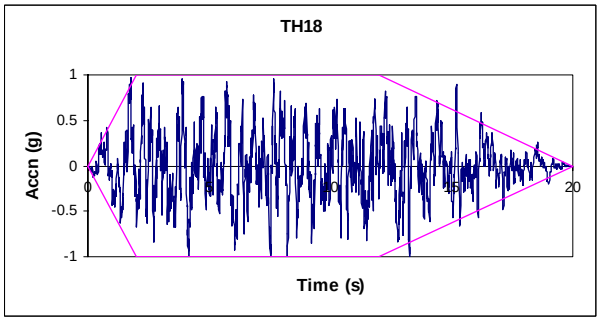
TH18
Accn (g)
Time (s)

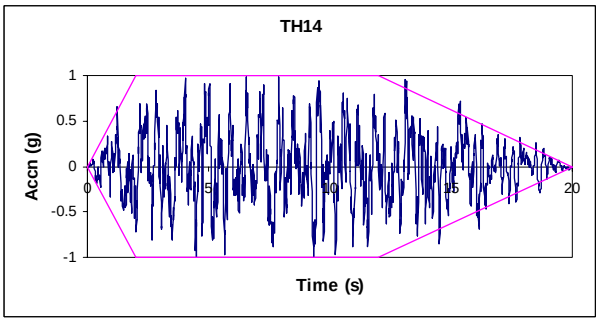
TH14
Accn (g)
Time (s)

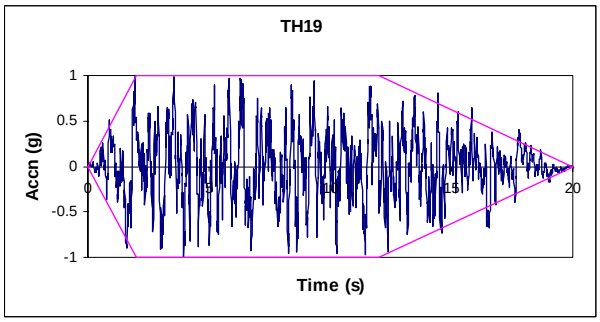
TH19
Accn (g)
Time (s)

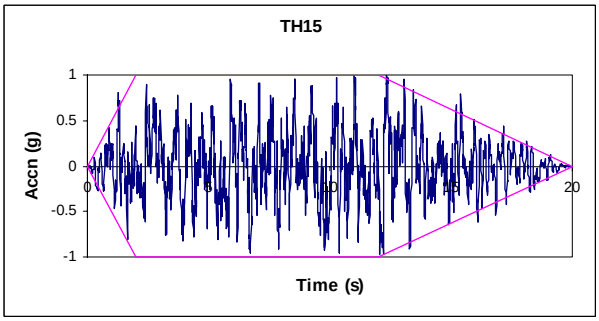
TH15
Accn (g)
Time (s)

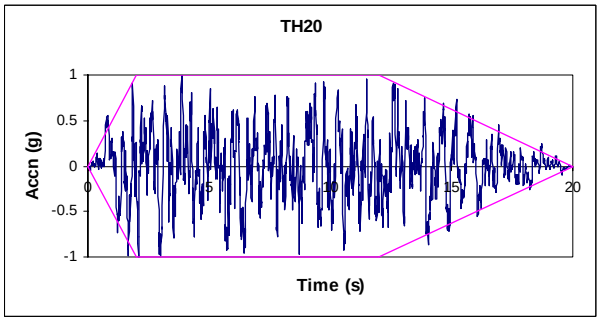
TH20
Accn (g)
Time (s)

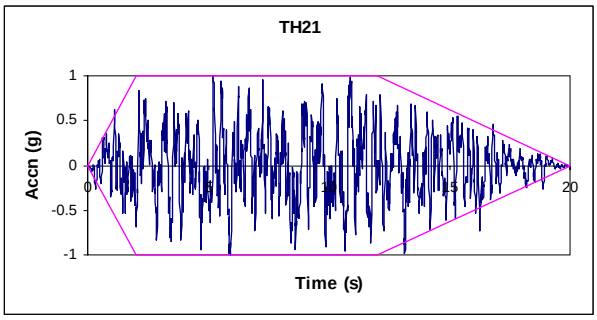
TH21
Accn (g)
Time (s)

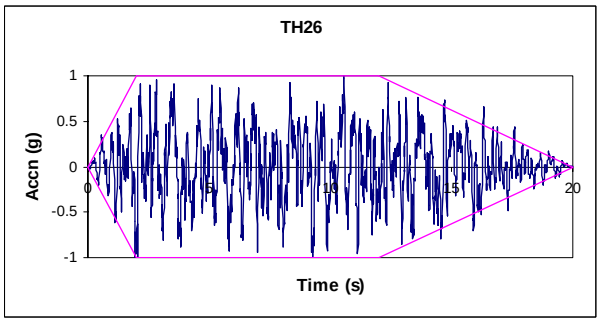
TH26
Accn (g)
Time (s)

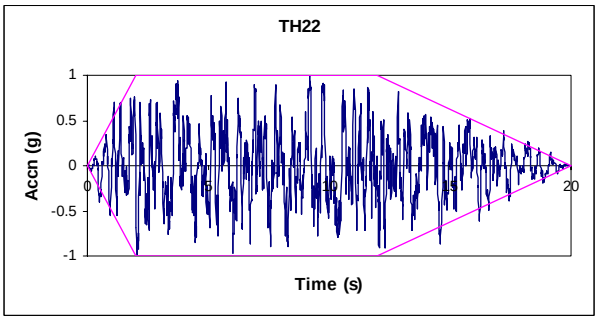
TH22
Accn (g)
Time (s)

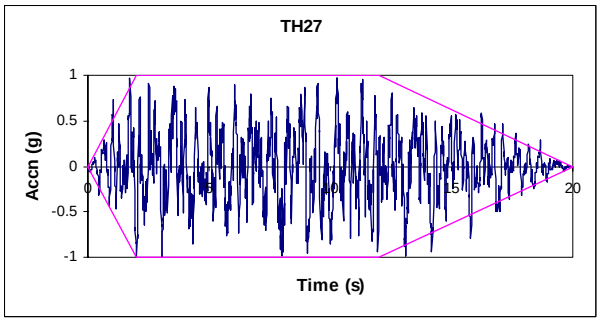
TH27
Accn (g)
Time (s)

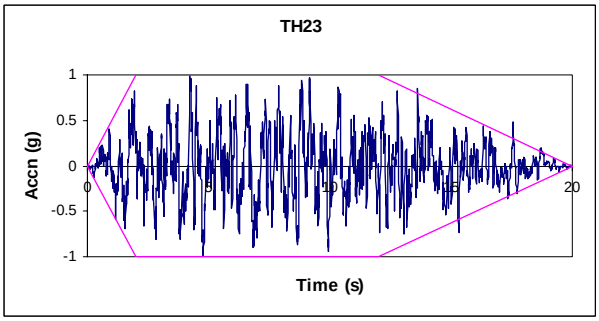
TH23
Accn (g)
Time (s)

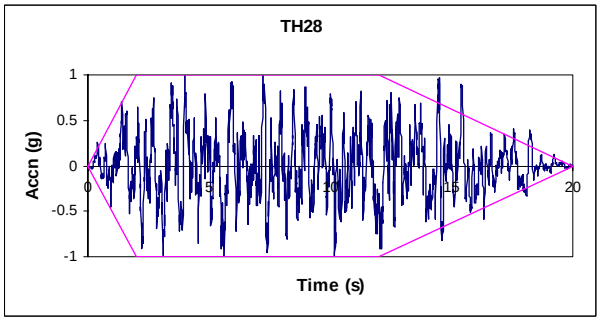
TH28
Accn (g)
Time (s)

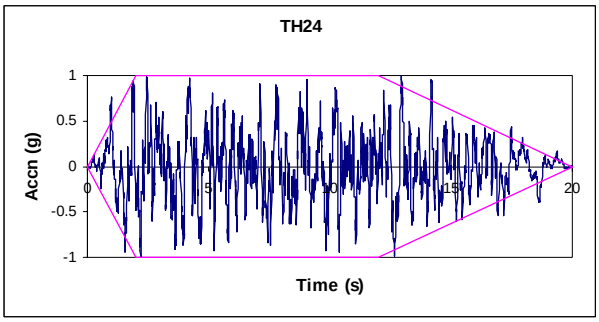
TH24
Accn (g)
Time (s)

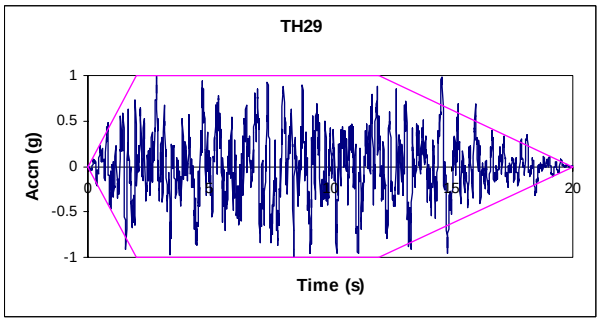
TH29
Accn (g)
Time (s)

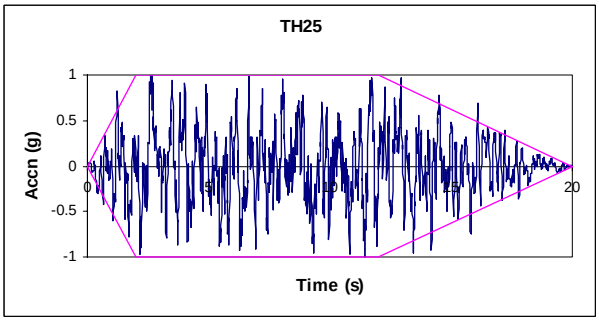
TH25
Accn (g)
Time (s)

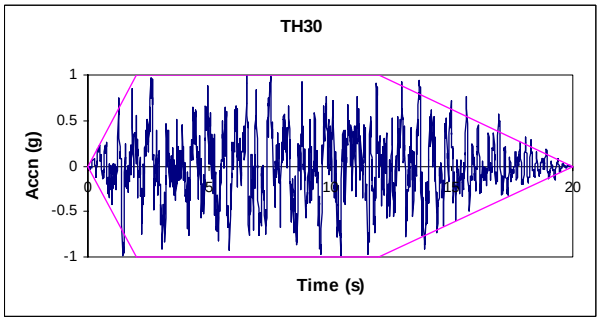
TH30
Accn (g)
Time (s)

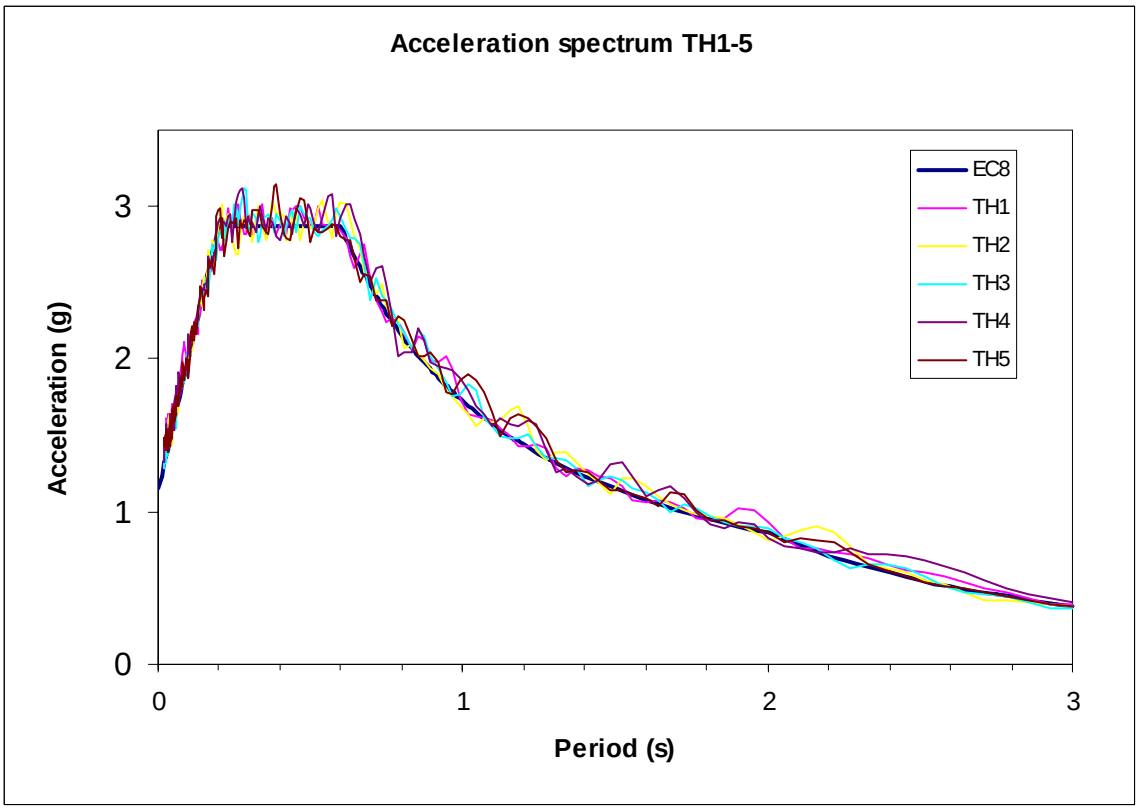
Acceleration spectrum TH1-5
Acceleration (g)
Period (s)
EC8
TH1
TH2
TH3
TH4
TH5
0
1
2
3

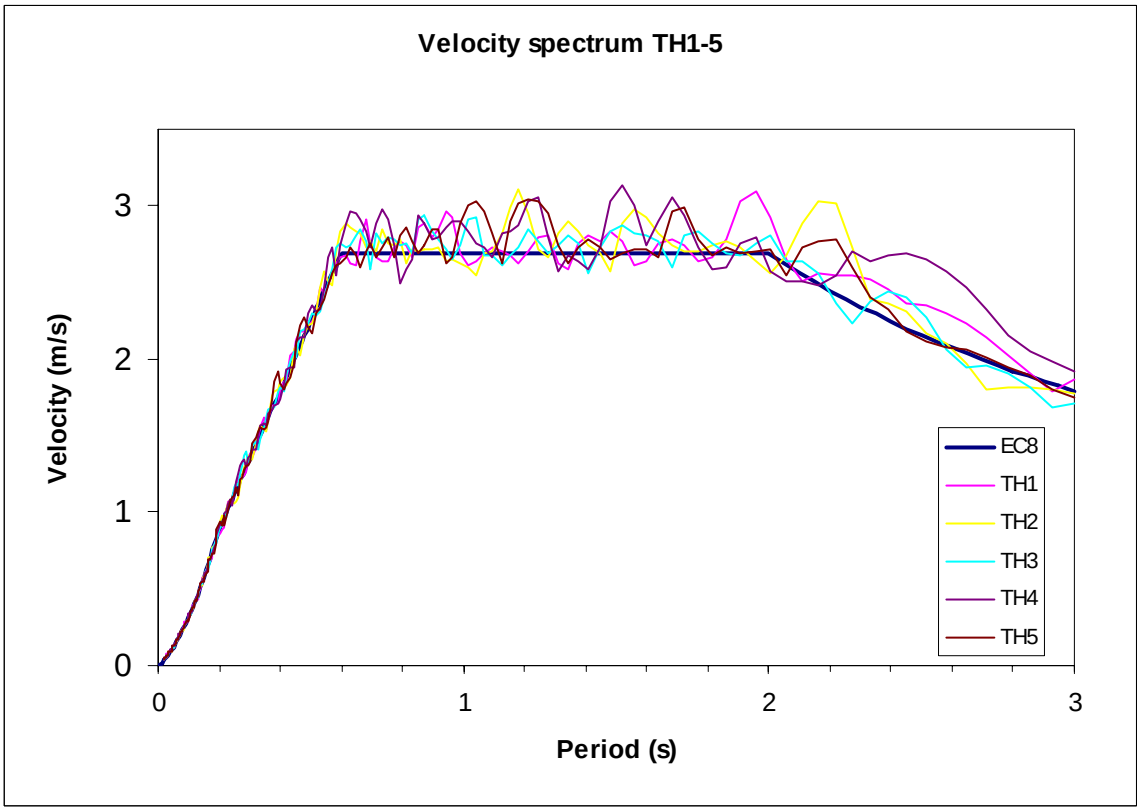
Velocity spectrum TH1-5
Velocity (m/s)
Period (s)
EC8
TH1
TH2
TH3
TH4
TH5
0
1
2
3

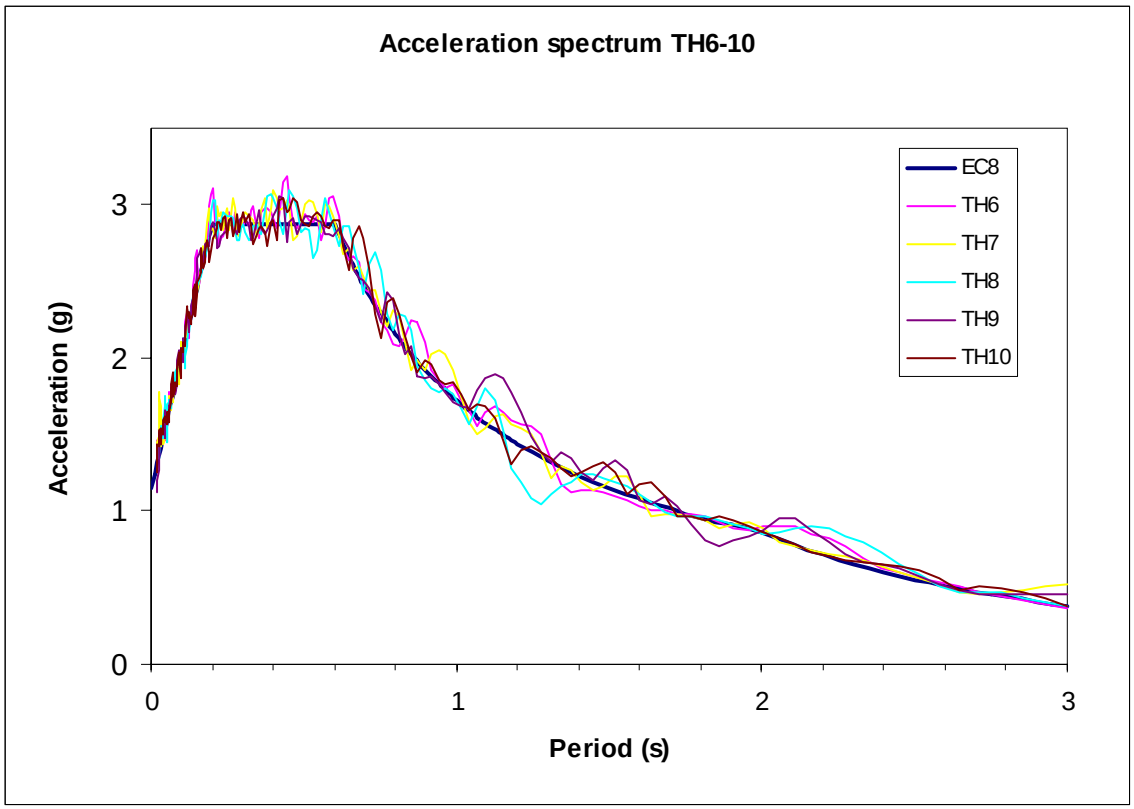
Acceleration spectrum TH6-10
Acceleration (g)
Period (s)
EC8
TH6
TH7
TH8
TH9
TH10
0
1
2
3

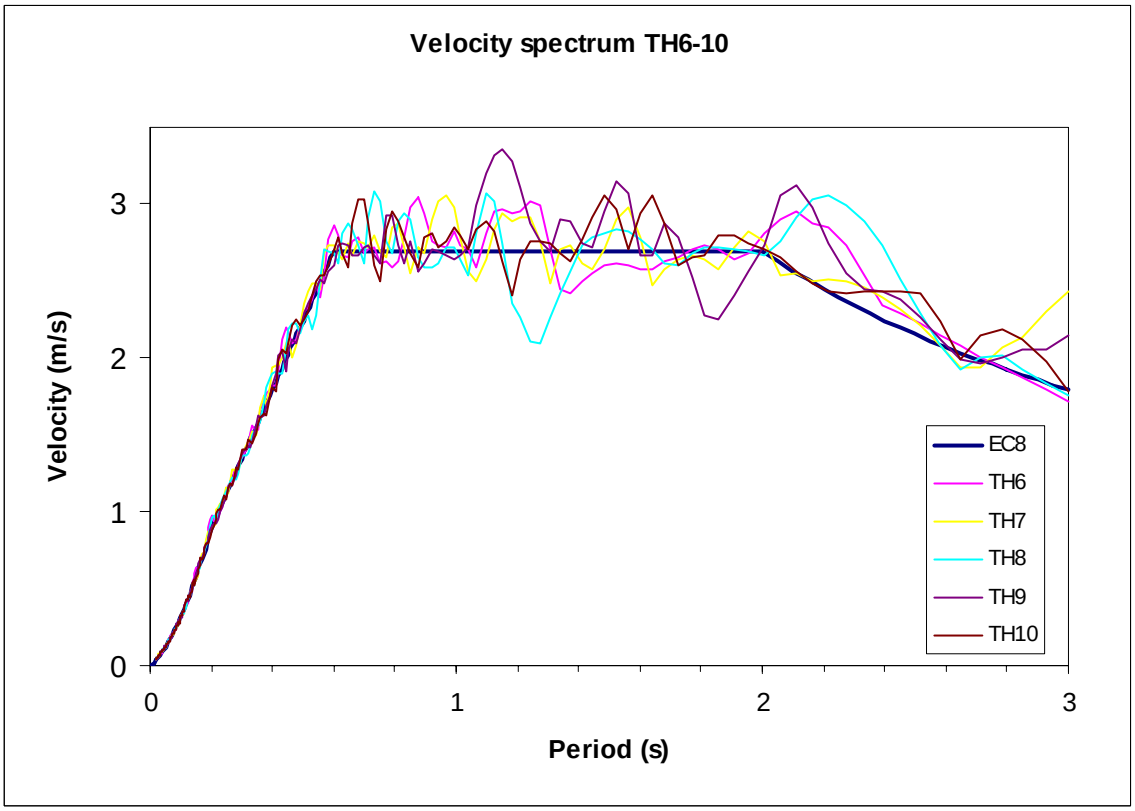
Velocity spectrum TH6-10
Velocity (m/s)
Period (s)
EC8
TH6
TH7
TH8
TH9
TH10
0
1
2
3

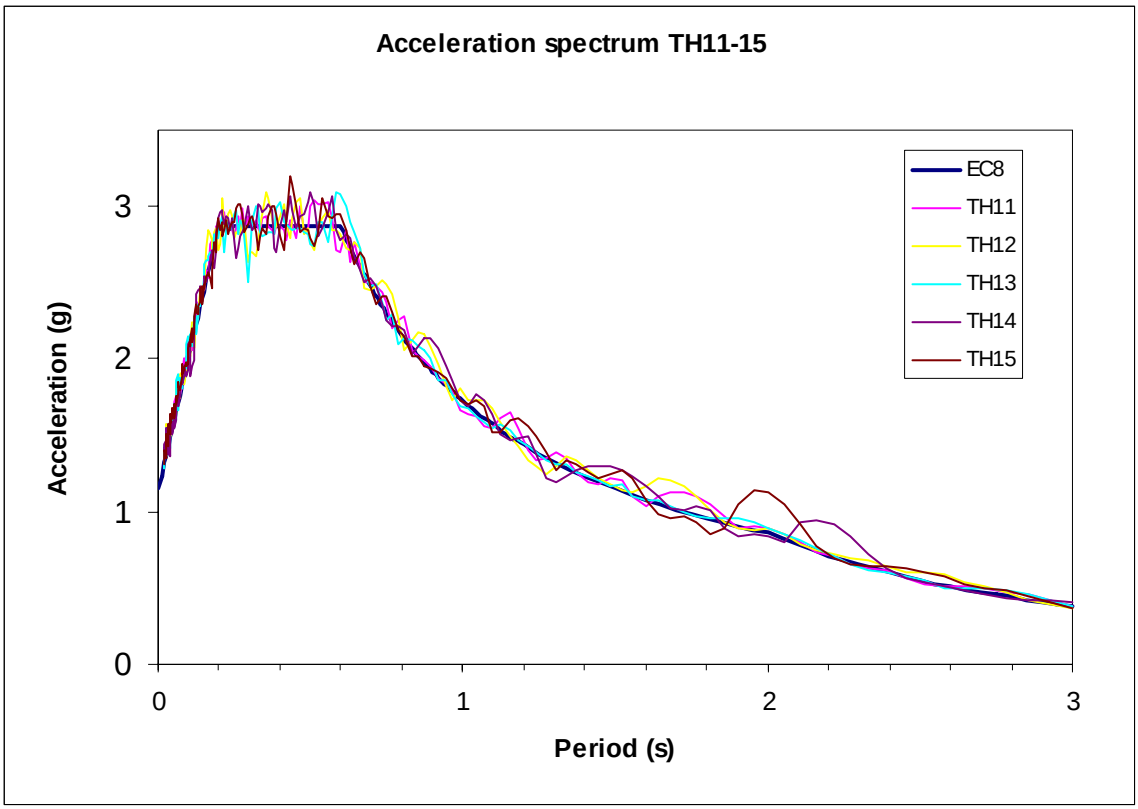
Acceleration spectrum TH11-15
Acceleration (g)
Period (s)
EC8
TH11
TH12
TH13
TH14
TH15
0
1
2
3

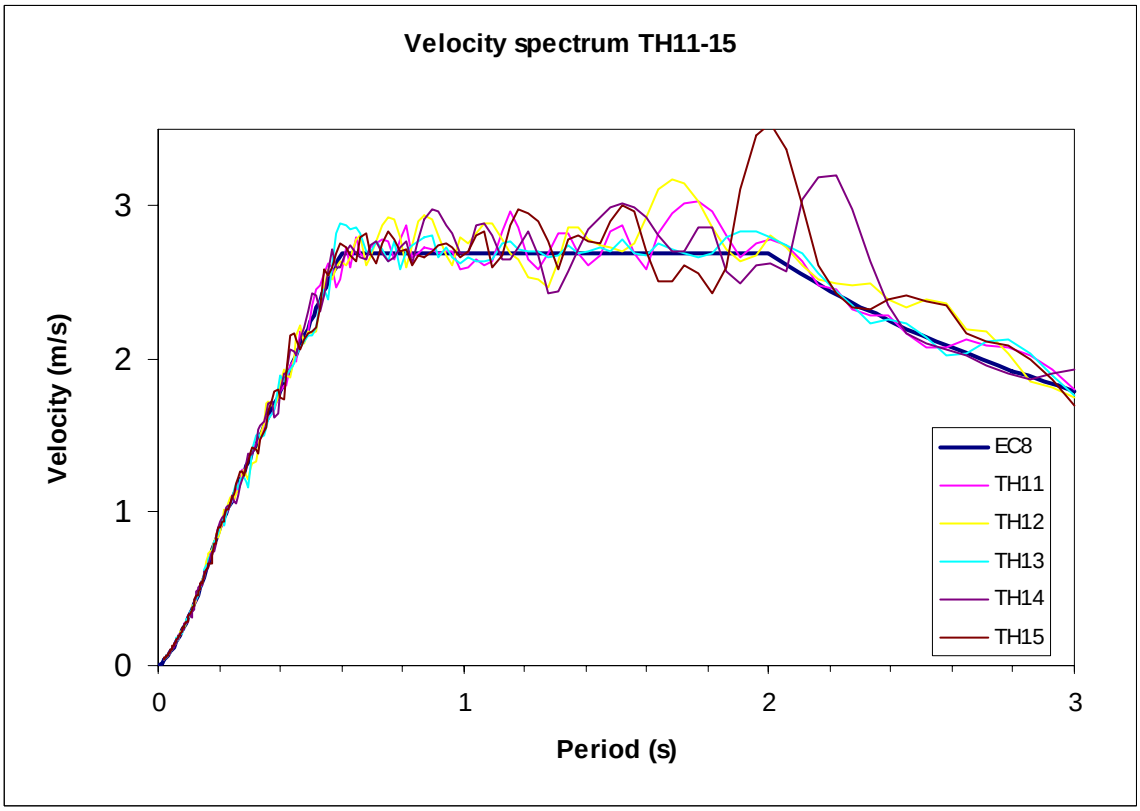
Velocity spectrum TH11-15
Velocity (m/s)
Period (s)
EC8
TH11
TH12
TH13
TH14
TH15
0
1
2
3

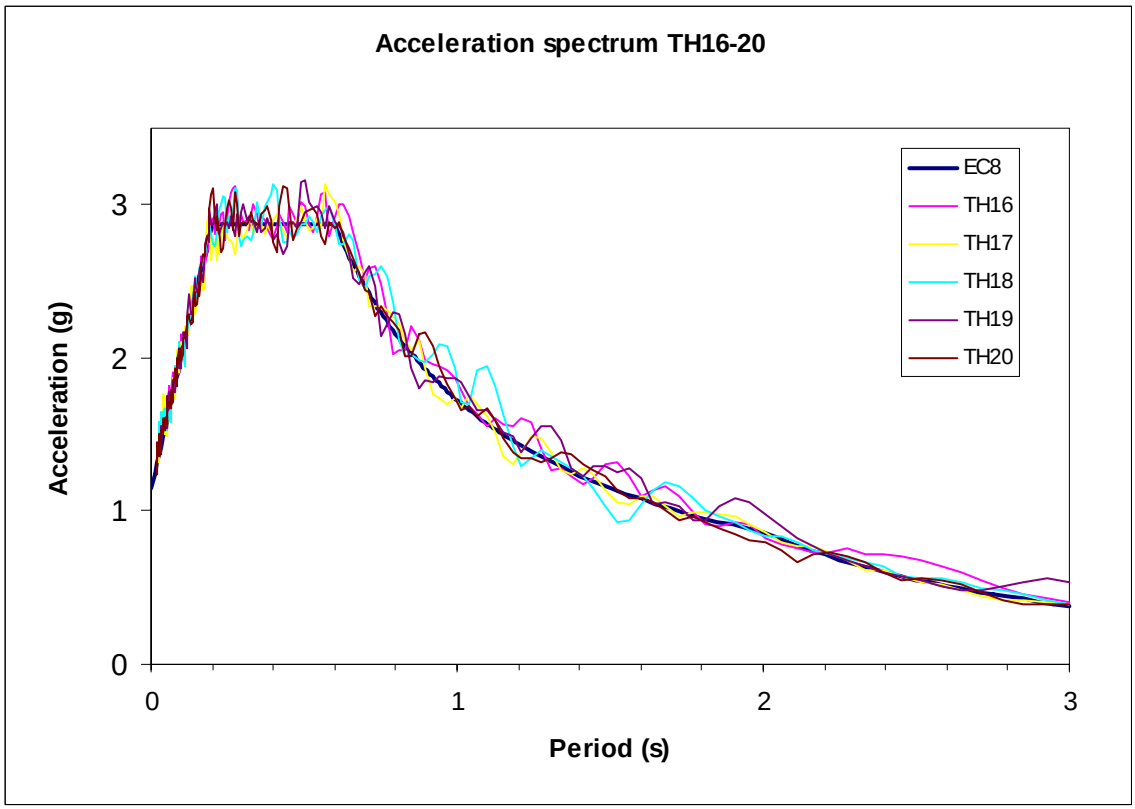
Acceleration spectrum TH16-20
Acceleration (g)
Period (s)
EC8
TH16
TH17
TH18
TH19
TH20
0
1
2
3

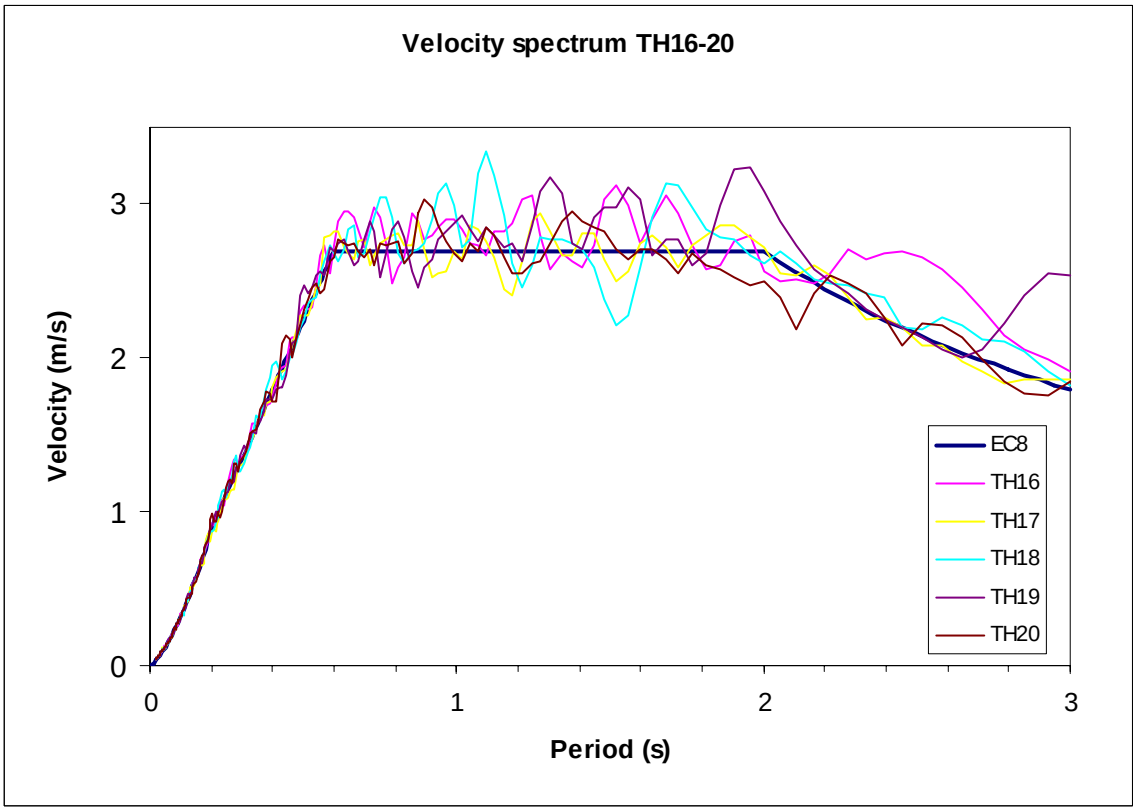
Velocity spectrum TH16-20
Velocity (m/s)
Period (s)
EC8
TH16
TH17
TH18
TH19
TH20
0
1
2
3

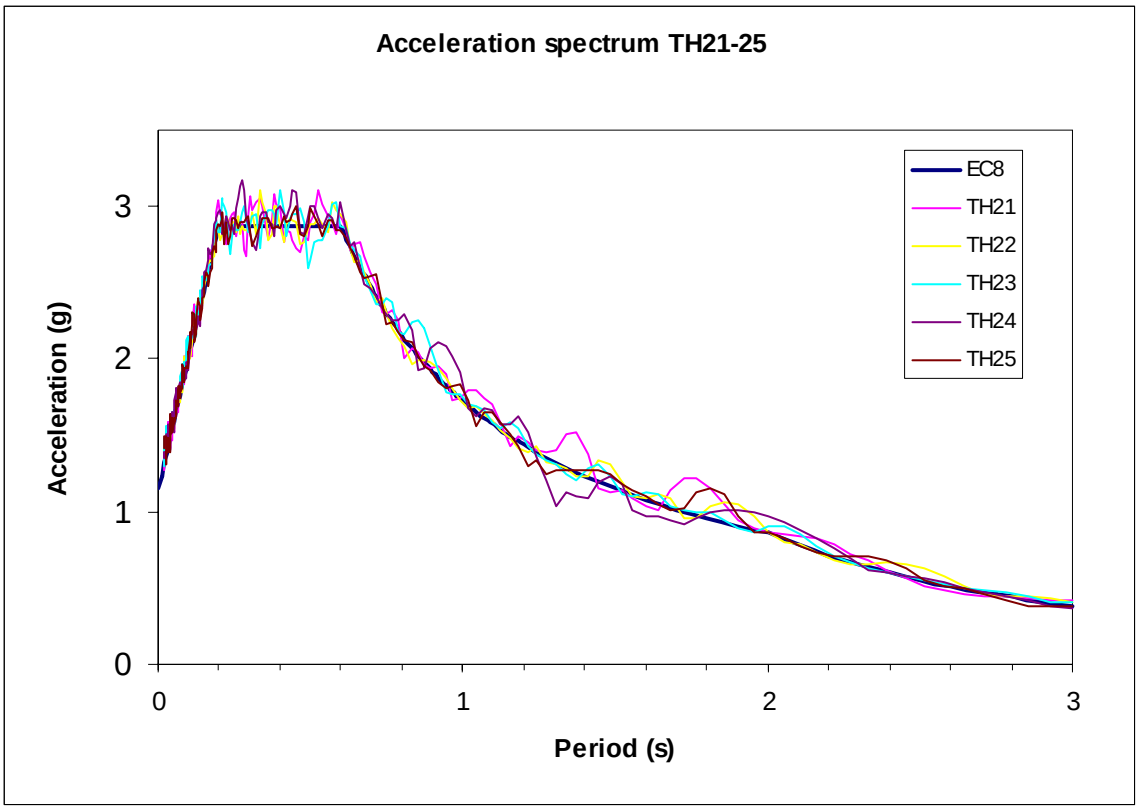
Acceleration spectrum TH21-25
Acceleration (g)
Period (s)
EC8
TH21
TH22
TH23
TH24
TH25
0
1
2
3

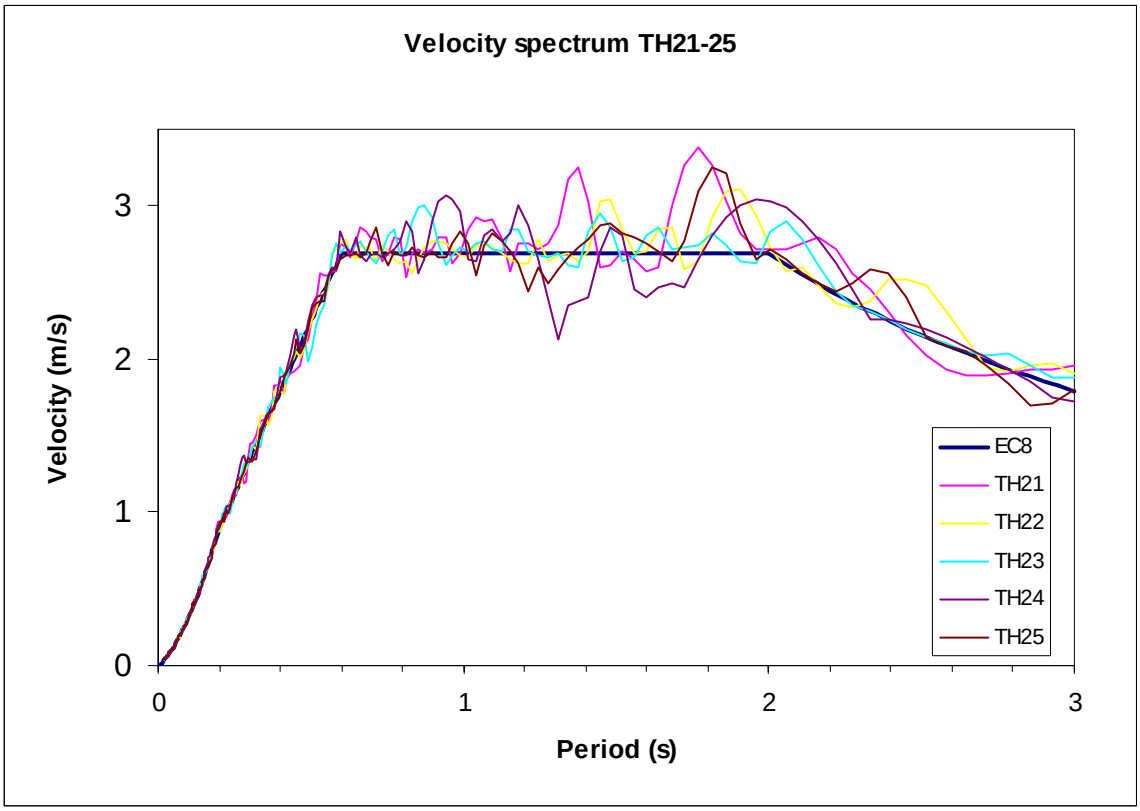
Velocity spectrum TH21-25
Velocity (m/s)
Period (s)
EC8
TH21
TH22
TH23
TH24
TH25
0
1
2
3

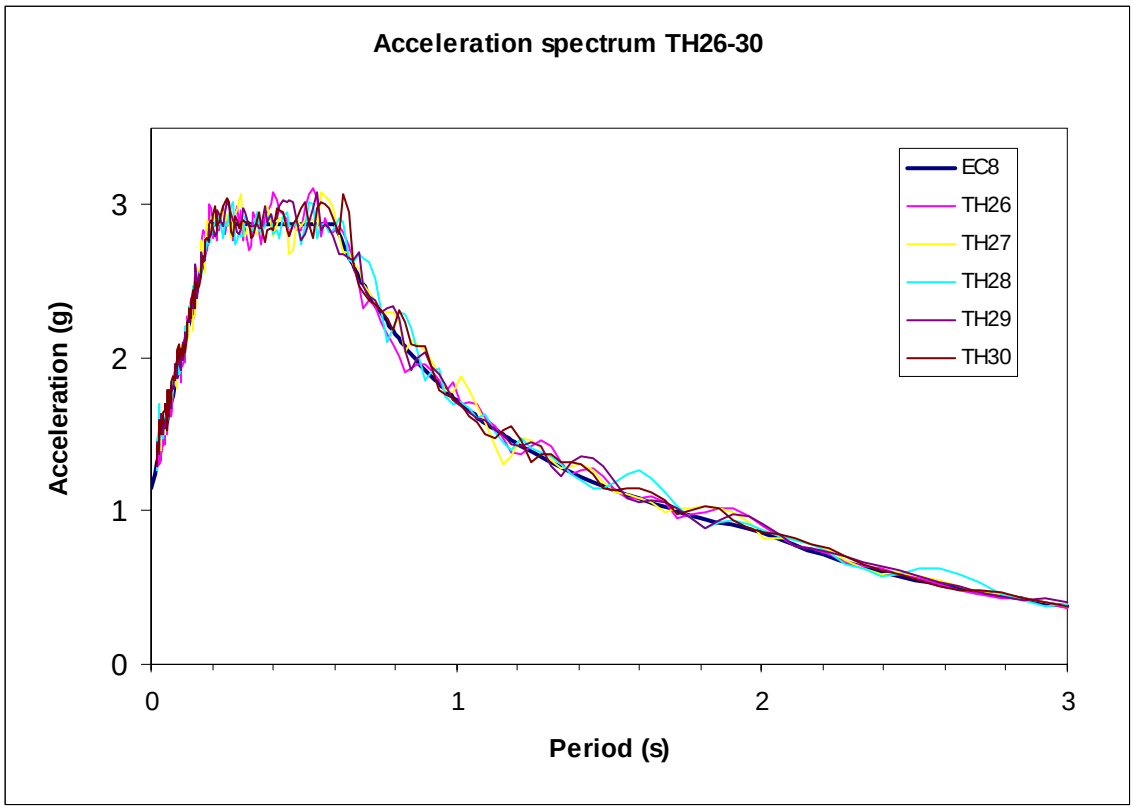
Acceleration spectrum TH26-30
Acceleration (g)
Period (s)
EC8
TH26
TH27
TH28
TH29
TH30
0
1
2
3

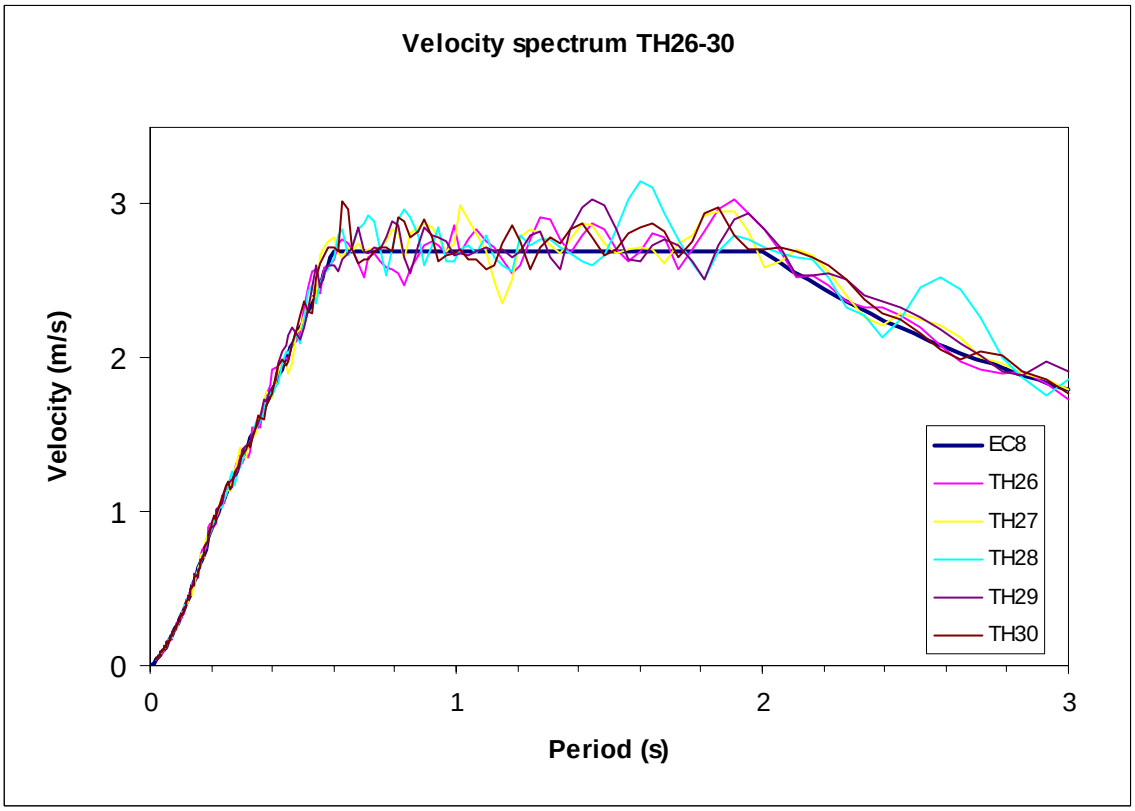
Velocity spectrum TH26-30
Velocity (m/s)
Period (s)
EC8
TH26
TH27
TH28
TH29
TH30
0
1
2
3